

Solving fractional differential equations of variable-order involving operators with Mittag-Leffler kernel using artificial neural networks



C.J. Zúñiga-Aguilar^a, H.M. Romero-Ugalde^b, J.F. Gómez-Aguilar^{c,*}, R.F. Escobar-Jiménez^a, M. Valtierra-Rodríguez^d

^aCentro Nacional de Investigación y Desarrollo Tecnológico, Tecnológico Nacional de México, Interior Internado Palmira S/N, Col. Palmira, C.P. 62490, Cuernavaca, Morelos, México

^bUniversity Grenoble Alpes, F-38000 Grenoble, France, CEA LETI MINATEC Campus, F-38054 Grenoble France

^cCONACyT - Centro Nacional de Investigación y Desarrollo Tecnológico, Tecnológico Nacional de México, Interior Internado Palmira S/N, Col. Palmira, C.P. 62490, Cuernavaca, Morelos, México

^dFacultad de Ingeniería, Universidad Autónoma de Querétaro, Campus San Juan del Río, Río Moctezuma 249, Col. San Cayetano, C.P. 76807, México

ARTICLE INFO

Article history:

Received 14 April 2017

Revised 28 June 2017

Accepted 28 June 2017

Available online 5 July 2017

Keywords:

Fractional calculus

Nonlinear fractional differential equations

Atangana-Baleanu-Caputo fractional derivative

Variable-order fractional derivative

Artificial neural networks

ABSTRACT

In this paper, we approximate the solution of fractional differential equations using a new approach of artificial neural network. We consider fractional differential equations of variable-order with Mittag-Leffler kernel in Liouville–Caputo sense. With this new neural network approach, it is obtained an approximate solution of the fractional differential equation and this solution is optimized using the Levenberg–Marquardt algorithm. The neural network effectiveness and applicability were validated by solving different types of fractional differential equations, the Willamowski–Rössler oscillator and a multi-scroll system. The solution of the neural network was compared with the analytical solutions and the numerical simulations obtained through the Adams–Bashforth–Moulton method. To show the effectiveness of the proposed neural network different performance indices were calculated.

© 2017 Elsevier Ltd. All rights reserved.

1. Introduction

Fractional calculus (FC) is a generalization of integration and differentiation to non-integer order. Recent studies in science and engineering demonstrated that the dynamics of many systems can be described more accurately by means of differential equations of non-integer order, for instance bioengineering, viscoelasticity, diffusion, chaos theory, physics, electromagnetism, and many others [1–8]. There are several approximation techniques to solve nonlinear fractional partial differential equations. In general, we can use direct and indirect implementation techniques for numerical approximation of the fractional operator, several numerical and analytical methods have been developed, for example, fractional sub-equation method [9–11], the homotopy perturbation method [12–14], the variational iteration method [15–18], homotopy perturbation transform method [19–21], Adomian decomposition method [22–24], Wavelet Method [25,26], Laplace transforms [27,28]. Several definitions of fractional order derivatives have been proposed, including: Grünwald–Letnikov, Riemann–Liouville, Weyl, Riesz and

the Liouville–Caputo representation. In 2016 Atangana and Baleanu presented another version of fractional derivatives, which uses the generalized Mittag-Leffler function as the non-singular and non-local kernel. This definition has all the benefits of the fractional operators of Riemann–Liouville or Liouville–Caputo [29–32]. Several studies have shown that, many complex physical problems can be described with great success via variable-order derivatives (VO), [33–36]. A novel study underlining the advantages of using these derivatives rather than constant order fractional derivative was presented in [37]. Some applications include processing of geographical data, diffusion processes and groundwater flow equation [38–40]. The equations described by the VO derivatives are highly complex, difficult to handle analytically, it is therefore advisable to research their solutions numerically [41–43]. In [43], the authors proposed a modification to the ABM method to solve differential equations of fractional order in Liouville–Caputo sense. The integration step is function of the delay and the number of samples. The authors showed that the numerical errors decay quickly by reducing the integration step size.

Artificial neural networks (ANNs) have also been successfully applied on many scientific and engineering fields thanks to their robustness [44] and their capacity to approximate nonlinear behaviors or functions. Cybenko established in [45] that a nonlinear

* Corresponding author.

E-mail addresses: jgomez@cenidet.edu.mx, jfranciscogoma@hotmail.com (J.F. Gómez-Aguilar).

function $f(x, u)$ can be approximated through the sum of sigmoidal or smooth functions [46]. Among the applications of ANNs, we found nonlinear system identification [47,48], ANNs-based control systems [49,50], and classification [51,52]. ANNs have been used to find the solution of fractional differential equations (FDEs) with the purpose of optimizing integration techniques. In [53] an ANN was proposed to solve FDEs with nonlinear behavior by using gradient-based algorithms. Although the initial conditions (solutions) found by the ANNs were not exactly the same than those found analytically, accurate results were obtained with a small number of neurons. Jafarian in [54] presented an ANN approach for solving a class of FDEs. The authors used an unsupervised back-propagation learning algorithm for adjusting the synaptic weights of the ANN and a suitable truncated power series of the solution function. In [55], a stochastic technique for solving the non-integer order Riccati differential equation was presented. A Feed-forward ANN was employed for accurate mathematical modeling. The training was performed by a heuristic computational algorithm based on swarm intelligence. A feed-forward artificial neural network was also used in [56] to find the solution of the a fractional order system represented by Bagley-Torvik equation. The synaptic weights optimization was made by using an evolutionary intelligence algorithm based on a genetic algorithm combined with a pattern search technique. Raja presented in [57] a new computational intelligence technique based on ANNs and sequential quadratic programming (SQP). This technique was applied on the solution of non-linear quadratic Riccati differential equations of fractional order. In [58] Kashkaria and Syam apply numerical treatment, for a class of non-linear Volterra-Fredholm integro-differential equations, using evolutionary intelligence. The authors presented comparisons of the proposed method and the analytical solutions. One of the important advantages of ANNs for function approximation is that the solution of differential equations is presented as a differentiable function. Although the ANNs are trained on a number of points, the solution can be calculated at each arbitrary point in the training interval even between training points. Recently, in [59], the authors proposed a simple structure for optimizing, through Quasi-Newton, the FDEs solutions. The proposed method considers the initial conditions and the order of the differential equation to improve the solution. These results obtained showed promising to solve nonlinear FDEs (NLFDE). However, if the degree of complexity considerably increases, the proposed neural network structure is not capable of finding the differential equation solution.

The application of fractional derivatives of Atangana-Baleanu with variable-order has not been reported in the literature yet. Therefore, in this paper, we deal with the solution of the FDE by using a new neural network approach. This approach allows solving multi-terms of the FDEs. Simulation examples for evaluating the proposed approach include non-linear FDEs, the Willamowski-Rössler oscillator and a chaos generator (2D-grid scroll attractor family). The manuscript is organized as follows: in Section 2, we recall the fractional operators. Section 3 presents the proposed ANN and the solution method. Section 4 presents the numerical results, the comparison made with others numerical methods and the performance indicators obtained based on the different values of fractional order. Finally, Section 5 is devoted to our conclusions.

2. Preliminaries and notation

Definition 1. Let $f \in \mathbb{R}[a, b]$, $b > a$, $\alpha \in [0, 1]$ then, the definition of the Liouville-Caputo fractional derivative is given as

$$({}_{t_0}^C \mathcal{D}_t^\alpha f)(t) = \frac{1}{\Gamma(1-\alpha)} \int_{t_0}^t \frac{f'(\tau)}{(t-\tau)^\alpha} d\tau, \quad n-1 < \alpha \leq n, \quad (1)$$

where $\Gamma(\cdot)$ denotes the Gamma function.

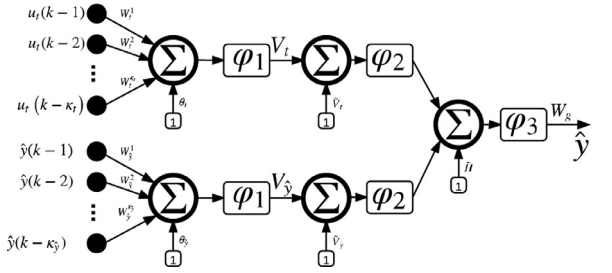


Fig. 1. Three layer artificial neural network proposed for solving variable order FDEs. The architecture is composed of two neurons in the first layer, two neurons in the second layer, and one neuron in the output layer, i.e., a 2 - 2 - 1 neural network.

Definition 2. Let $f \in \mathbb{R}[a, b]$, $b > a$, $\alpha \in [0, 1]$ then, the definition of the Atangana-Baleanu fractional derivative in Liouville-Caputo sense (ABC) is given as

$$({}_{t_0}^{ABC} \mathcal{D}_t^\alpha f)(t) = \frac{B(\alpha)}{1-\alpha} \int_{t_0}^t \dot{f}(\tau) E_\alpha \left[-\alpha \frac{(t-\tau)^\alpha}{1-\alpha} \right] d\tau, \\ n-1 < \alpha(t) \leq n, \quad (2)$$

where $\alpha \in \mathbb{R}$, $B(\alpha)$ denotes a normalization function $B(0) = B(1) = 1$ and $E_\alpha(\cdot)$ denotes the Mittag-Leffler function.

Definition 3. The fractional integral associated to the ABC derivative with non-local kernel is defined as

$${}_{t_0}^{AB} I_t^\alpha \{f(t)\} = \frac{1-\alpha}{B(\alpha)} f(t) + \frac{\alpha}{B(\alpha)\Gamma(\alpha)} \int_{t_0}^t f(\tau) (t-\tau)^{\alpha-1} d\tau. \quad (3)$$

In Eq. (3), when α is equal to zero we recover the initial function and when $\alpha = 1$, we obtain the classical ordinary integral [29].

In the case when the fractional order is a time function given as $\alpha : \mathbb{R} \rightarrow \mathbb{R}$, $t \mapsto \alpha(t) \wedge \alpha = \{\alpha(t) : 0 < \alpha(t) \leq 1\}$, the derivative expressed in Eq. (2) becomes Eq. (4).

Definition 4. The definition of the variable-order derivative in the Atangana-Baleanu-Caputo sense can be formulated as follows

$$({}_{t_0}^{ABC} \mathcal{D}_t^{\alpha(t)} f)(t) = \frac{B(\alpha(t))}{1-\alpha(t)} \int_{t_0}^t \dot{f}(\tau) E_{\alpha(t)} \left[-\alpha(t) \frac{(t-\tau)^{\alpha(t)}}{1-\alpha(t)} \right] d\tau, \\ n-1 < \alpha(t) \leq n, \quad (4)$$

where $B(\alpha(t))$ is the normalization function defined by

$$B(\alpha(t)) = 1 - \alpha(t) + \frac{\alpha(t)}{\Gamma(\alpha(t))}. \quad (5)$$

Definition 5. The definition of the variable-order integral in the Atangana-Baleanu sense can be formulated as follows

$$({}_{t_0}^{AB} I_t^{\alpha(t)} f)(t) = \frac{1-\alpha(t)}{B(\alpha(t))} f(t) + \frac{\alpha(t)}{B(\alpha(t))\Gamma(\alpha(t))} \\ \times \int_{t_0}^t f(\tau) (t-\tau)^{\alpha(t)-1} d\tau, \quad n-1 < \alpha(t) \leq n. \quad (6)$$

Definition 6. The Adams method for Atangana-Baleanu-Caputo fractional derivative was described in [31], however, the order of the fractional derivative is constant. Now, in this paper we present a variation of this method using a variable-order. Thus, the algorithm calculates a numerical solution of a fractional differential equation of the form

$${}_{0}^{ABC} \mathcal{D}_t^{\alpha(t)} f(t) = g(t, f(t)), \quad f^k(0) = f_0^k, \quad k = 0, 1, \dots, n-1, \quad (7)$$

where $\alpha(t) > 0$ and ${}_{0}^{ABC} D_t^{\alpha(t)}$ is the Atangana-Baleanu-Caputo fractional derivative of variable-order.

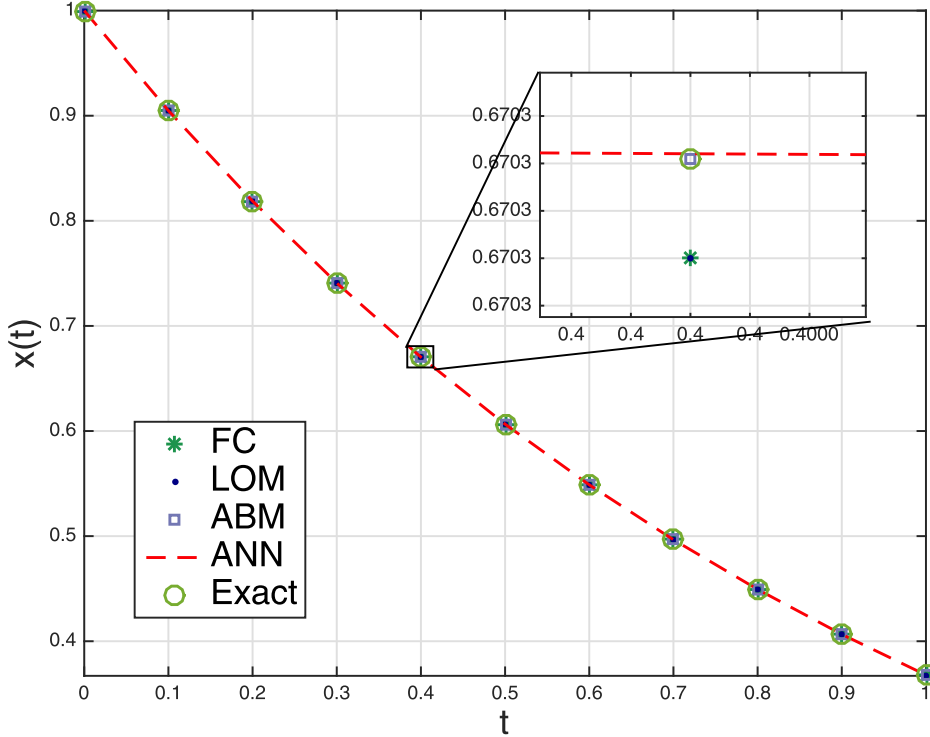


Fig. 2. The comparison between the ANN with other integration methods.

Eq. (7) has one solution defined in $t \in [0, T]$, this solution can be rewritten using the fractional Atangana-Baleanu integral as follows

$$f(t) = f_0 + \frac{1 - \alpha(t)}{B(\alpha(t))} g(t, f(t)) + \frac{\alpha(t)}{B(\alpha(t)) \Gamma(\alpha(t))} \times \int_0^t g(u, f(u)) (t-u)^{\alpha(t)-1} du, \quad (8)$$

where $B(\alpha(t))$ is a normalization function given by Eq. (5).

Now the solution scheme using the trapezoidal quadrature formula is derived as follows

$$\begin{aligned} f_{i+1}^P &= f_0 + \frac{1 - \alpha(t_{i+1})}{B(\alpha(t_{i+1}))} g(t_{i+1}, f_{i+1}) + \frac{\alpha(t_{i+1})}{\Gamma(\alpha(t_{i+1})) B(\alpha(t_{i+1}))} \\ &\quad \times \sum_{j=0}^i b_{j,i+1} g(t_j, f_j), \\ f_{i+1} &= f_0 + \frac{1 - \alpha(t_{i+1})}{B(\alpha(t_{i+1}))} g(t_{i+1}, f_{i+1}^P) + \frac{\alpha(t_{i+1})}{B(\alpha(t_{i+1}))} \\ &\quad \times \left[\frac{h^{\alpha(t_{i+1})}}{\Gamma(\alpha(t_{i+1}) + 2)} g(t_{i+1}, f_{i+1}^P) + \frac{h^{\alpha(t_{i+1})}}{\Gamma(\alpha(t_{i+1}) + 2)} \right. \\ &\quad \left. \times \sum_{j=0}^i a_{j,i+1} g(t_j, f_j) \right], \end{aligned} \quad (9)$$

$$\text{where } a_{j,i+1} = \begin{cases} i^{\alpha(t_{i+1})+1} - (i - \alpha(t_{i+1}))(i+1)^{\alpha(t_{i+1})}, & j=0, \\ (i-j+2)^{\alpha(t_{i+1})+1} + (i-j)^{\alpha(t_{i+1})+1} - 2(i-j+1)^{\alpha(t_{i+1})+1}, & 1 \leq j \leq i, \end{cases}$$

$$\text{and } b_{j,i+1} = \frac{h^{\alpha(t_{i+1})}}{\alpha(t_{i+1})} ((i+1-j)^{\alpha(t_{i+1})} - (i-j)^{\alpha(t_{i+1})}), \quad j=0, 1, 2, \dots, i.$$

The reader shall notice that, scheme given in Eq. (9) constitutes a new algorithm for the numerical approximation of Eq. (7) con-

sidering the Atangana-Baleanu-Caputo fractional derivative with variable-order.

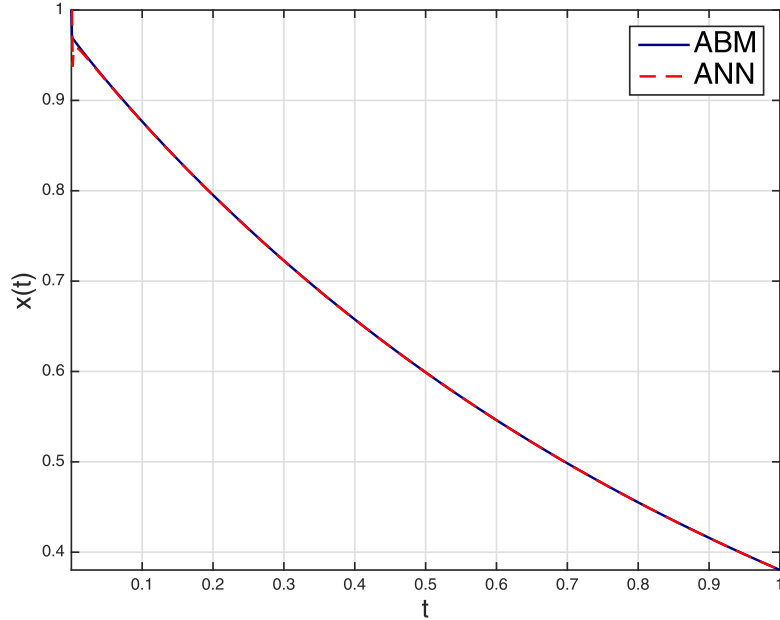
3. Proposed ANN for solving FDEs

The ANN used as basis in this work is presented in Fig. 1. This architecture, previously presented in [44–48], consists of a three layer recurrent neural network of two neurons in the first layer, two neurons in the second layer and one neuron in the output layer, i.e., a $2 - 2 - 1$ ANN. We can observe in Fig. 1, that each neuron is composed of a function (φ_i , with $i = 1, 2, 3$), processing the linear combination of the synaptic weights (model parameters, which may be optimized by a learning algorithm) and the inputs of the neuron. The output of each neuron is the input of another neuron of the ANN or the output of the ANN (when the neuron is in the output layer). The ANN used in this paper for solving FDEs (Fig. 1) is mathematically expressed by Eq. (10).

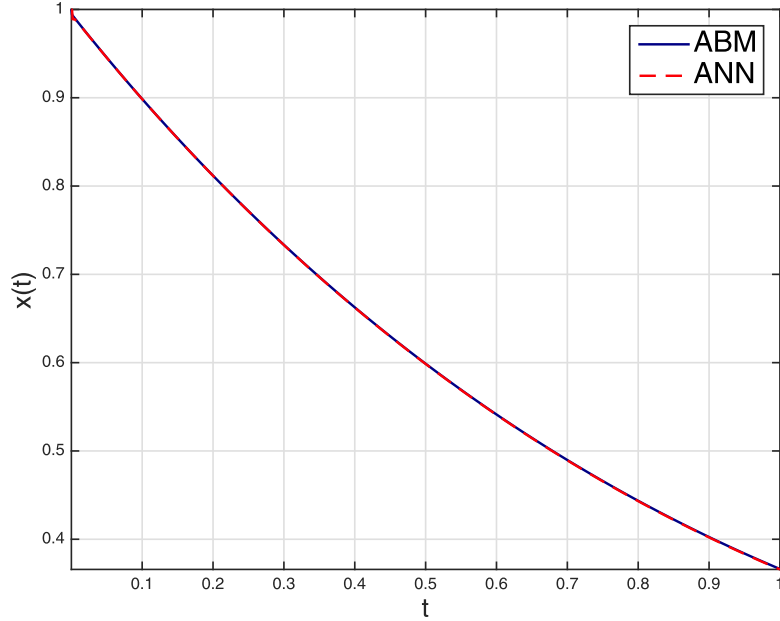
$$\hat{y} = W_g \varphi_3 (\varphi_2 (V_t \varphi_1 (J_t W_t + \theta_t) + \tilde{V}_t) + \varphi_2 (V_{\hat{y}} \varphi_1 (J_{\hat{y}} W_{\hat{y}} + \theta_{\hat{y}}) + \tilde{V}_{\hat{y}}) + \tilde{H}), \quad (10)$$

where functions φ_i , with $i = 1, 2, 3$, were classically chosen as $\varphi_3(z) = \varphi_2(z) = z$, $\varphi_1(z) = \tanh(z)$. In Eq. (10), $W_g, V_t, V_{\hat{y}} \in \mathbb{R}$, $W_t \in \mathbb{R}^{K_t}$, $W_{\hat{y}} \in \mathbb{R}^{K_{\hat{y}}}$, and $\theta_t, \theta_{\hat{y}} \in \mathbb{R}$ are the synaptic weights. Since φ_1 and φ_2 are linear functions, we can sum \tilde{V}_t , $\tilde{V}_{\hat{y}}$, and \tilde{H} as follows, i.e., $H_g = \tilde{V}_t + \tilde{V}_{\hat{y}} + \tilde{H} \in \mathbb{R}$, to reduce the number of parameters of the ANN. Finally, $J_t = [u_t(k-1) \ u_t(k-2) \ \dots \ u_t(k-K_t)] \in \mathbb{R}^{N \times K_t}$ and $J_{\hat{y}} = [\hat{y}(k-1) \ \hat{y}(k-2) \ \dots \ \hat{y}(k-K_{\hat{y}})] \in \mathbb{R}^{N \times K_{\hat{y}}}$ are regression matrix of time and output, respectively, where N is the number of data.

In the method proposed in [59] for solving FDEs, the initial value problem y_0 is fulfilled according to Eq. (11). The authors suppose that $\hat{y}_N(t, \Omega)$ is the solution of Eq. (11), where Ω is the synaptic



(a) Approximated solution with the ABM and ANN method with the fractional order $\alpha = 0.97$



(b) Approximated solution with the ABM and ANN method with the fractional variable-order $\alpha(t) = \tanh(3 - t)$

Fig. 3. Temporal solution for the Example 1.

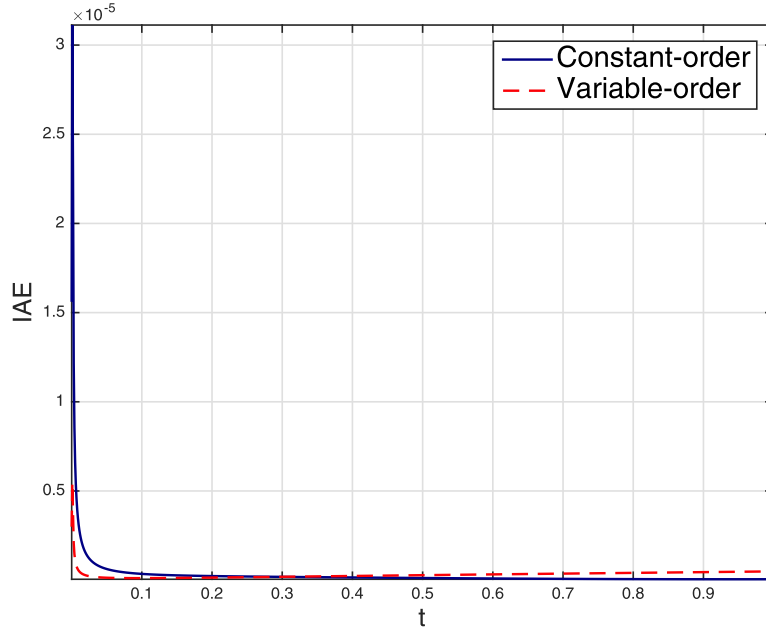
weights vector. Optimal parameters (Ω^*) leads $\hat{y}_N(t_0, \Omega^*) = y_0$.

$$(t_0 \mathfrak{D}_t^\alpha y)(t) = f(t, y)|_{t=t_0, y=y_0} = y_0. \quad (11)$$

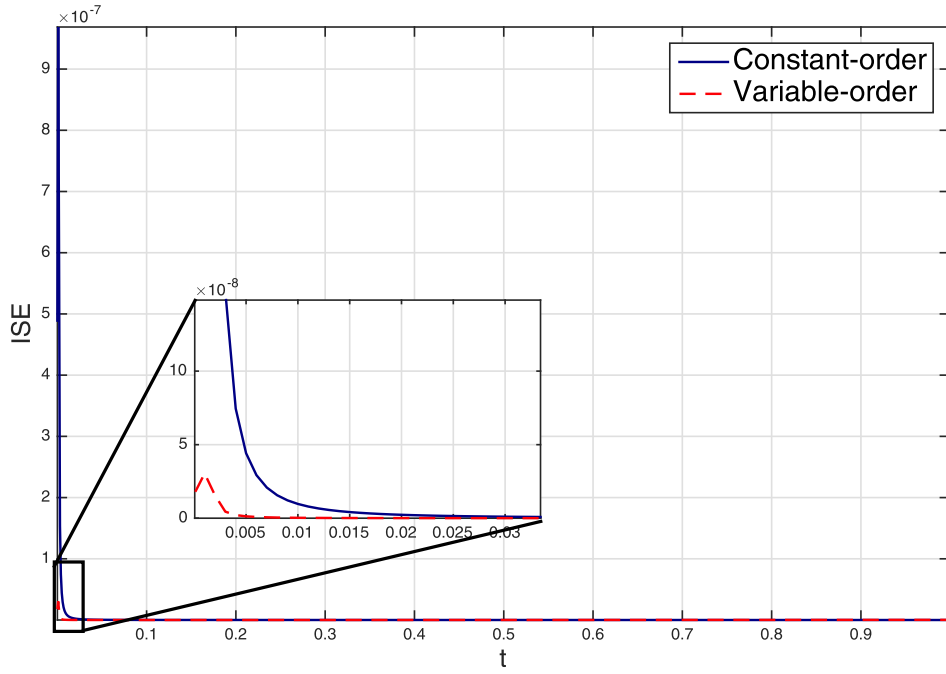
In this work, we proposed a solution depending on the initial condition and the neural network. This solution is given by

$$\hat{y}_N = y_0 + \sum_{j=1}^{\lceil \alpha(t) \rceil - 1} t^j + t^{\lceil \alpha(t) \rceil} \hat{y}(t, \Omega), \quad (12)$$

where $\lceil \alpha(t) \rceil$ is the upper integer value of $\alpha(t)$. As already mentioned, system identification is performed by the ANN showed in Fig. 1 and expressed in Eq. (10), which is able to approximate nonlinear functions. It is clear that Eq. (12) satisfies the initial condi-



(a) The integral of the absolute error for a constant and variable order.



(b) The integral of the square error for a constant and variable order.

Fig. 4. IAE and ISE performance indices.

tion of the FDE evaluating the Eq. (12) in an instant of time t_0 , now, replacing the Eq. (12) into Eq. (11) we have

$$\left({}_{t_0}^{ABC} \mathfrak{D}_t^{\alpha(t)} \hat{y}_N \right)(t, \Omega) = f(\hat{y}_N(t, \Omega), \tau), \quad (13)$$

where, the fractional operator ${}_{t_0}^{ABC} \mathfrak{D}_t^{\alpha(t)} y(t)$ can be of the type ABC with variable-order, i.e., ${}_{t_0}^{ABC} \mathfrak{D}_t^{\alpha(t)} y(t)$.

In fact, Eq. (13) is an optimization problem

$$\Omega^* = \min_{\Omega} \{ \Phi(e) \} = \min_{\Omega} \left\{ \frac{1}{2} \sum_{i=1}^N e_i^2 \right\}, \quad (14)$$

where $e := \left({}_{t_0}^{ABC} \mathfrak{D}_t^{\alpha(t)} \hat{y}_N \right)(t, \Omega) - f(\hat{y}_N(t, \Omega), \tau)$. Now, to approximate the fractional derivative showed in the Eq. (13), the Atangana-Baleanu-Caputo derivative of variable-order given in

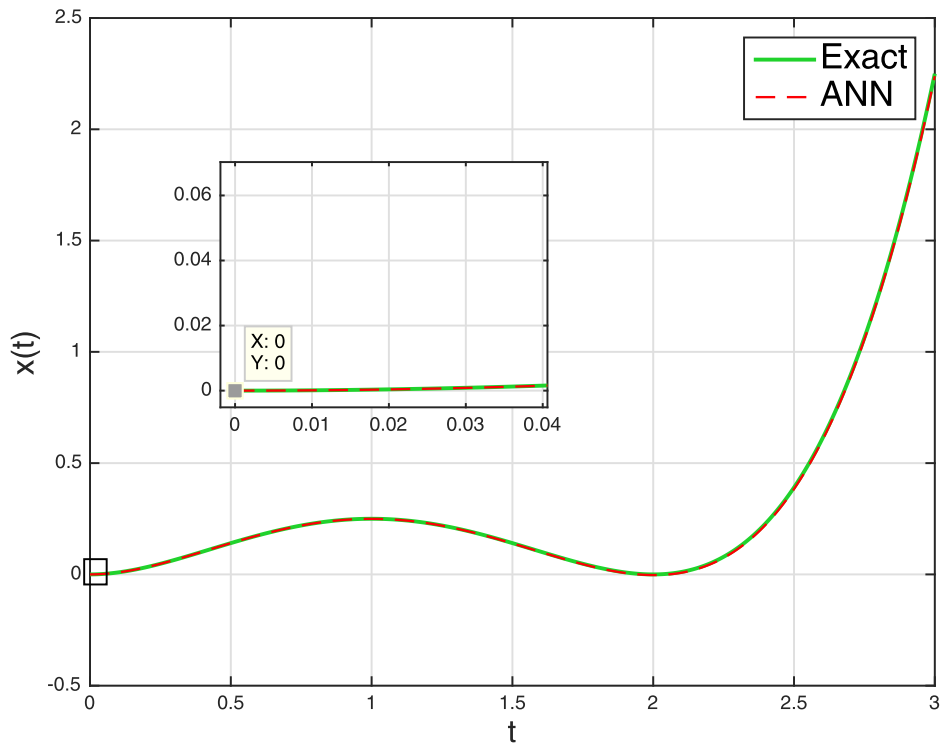


Fig. 5. Comparison between the ANN and the exact solution of the FDE given by Eq. (35).

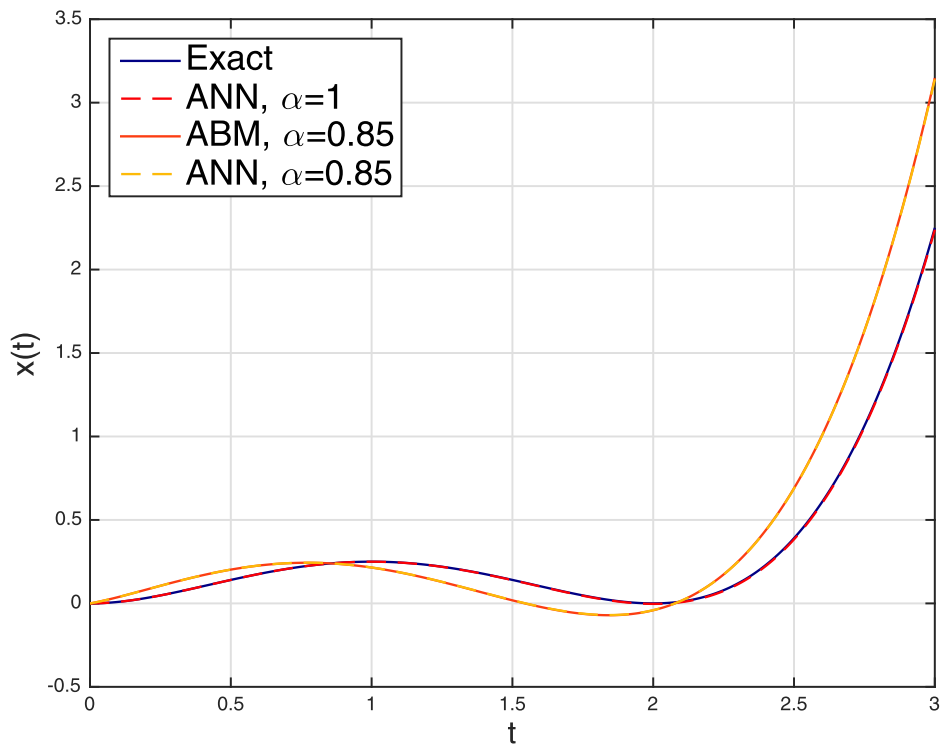


Fig. 6. Comparison between the ANN and ABM method for the fractional order $\alpha = 0.85$.

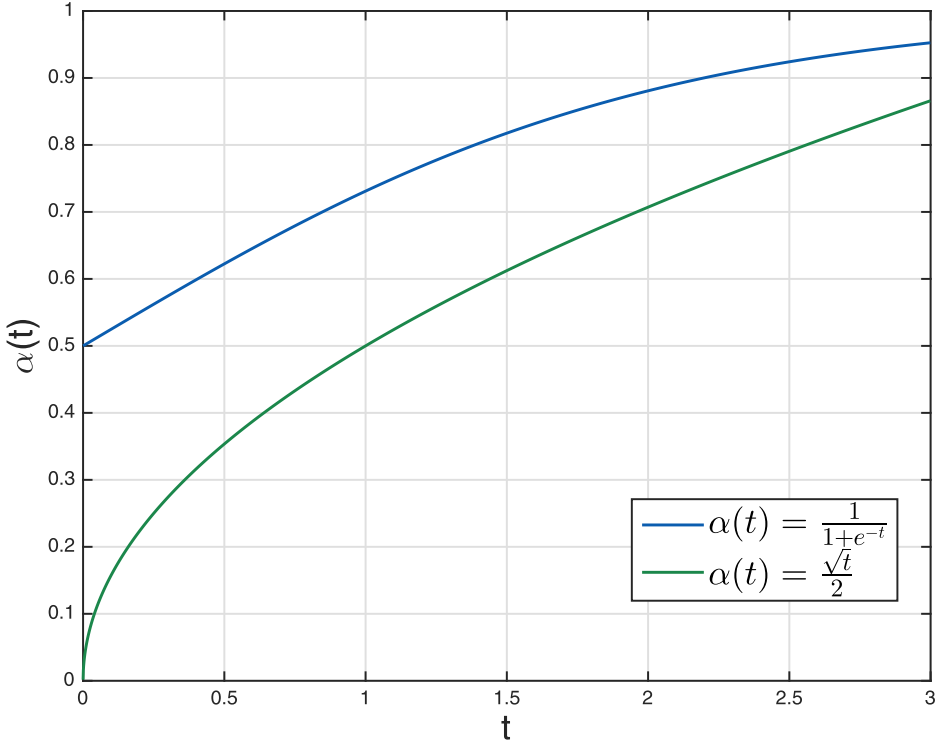


Fig. 7. Numerical simulations obtained with the fractional variable-order $\alpha(t) = \frac{1}{1+e^{-t}}$ and $\alpha(t) = \frac{\sqrt{t}}{2}$ in an interval of $t \in [0, 3]$.

Eq. (4) is used, such that

$$\begin{aligned} \left({}_{t_0}^{ABC} \mathfrak{D}_t^{\alpha(t)} \hat{y}_N \right)(t, \Omega) &= \frac{B(\alpha(t))}{1-\alpha(t)} \int_{t_0}^t \dot{\hat{y}}_N(\tau, \Omega) E_{\alpha(t)} \\ &\times \left[-\alpha(t) \frac{(t-\tau)^{\alpha(t)}}{1-\alpha(t)} \right] d\tau, \quad 0 < \alpha(t) \leq 1. \end{aligned} \quad (15)$$

The integral in Eq. (15) can be approximated by any numerical integration method, for instance, the trapezoidal method. But first, a change of variable is made for simplicity,

$$P(\alpha, \tau, \Omega, t) = \dot{\hat{y}}_N(\tau, \Omega) E_{\alpha(t)} \left[-\alpha(t) \frac{(t-\tau)^{\alpha(t)}}{1-\alpha(t)} \right]. \quad (16)$$

In consequence we have

$$f_p(t, \Omega) = \frac{B(\alpha(t))}{1-\alpha(t)} \int_{t_0}^t P(\alpha, \tau, \Omega, t) d\tau, \quad (17)$$

By using the trapezoidal method with height $h = \frac{t}{N}$, we have

$$\begin{aligned} f_p(t, \Omega) &\approx \frac{B(\alpha(t))h}{2(1-\alpha(t))} [P(\alpha, \tau, \Omega, 0) + 2P(\alpha, \tau, \Omega, h) \\ &+ \dots + 2P(\alpha, \tau, \Omega, (N-1)h) + P(\alpha, \tau, \Omega, t)]. \end{aligned} \quad (18)$$

According to Eq. (18), we have a new optimization problem

$$\Omega^* = \min_{\Omega} \left\{ \frac{1}{2} \sum_{k=1}^N (f_p(t_k, \Omega) - f(\hat{y}_N(t_k, \Omega), t_k))^2 \right\}. \quad (19)$$

Synaptic weights optimization is performed by the Levenberg-Marquardt (LM) algorithm, in order to minimize Eq. (19). For instance, the iterative procedure for optimizing an unknown synaptic weight is shown in Eq. (20).

$$\Delta W_k = [J(W_k)^T J(W_k) + \mu I]^{-1} J(W_k) (f_p(t_k, \Omega) - f(\hat{y}_N(t_k, \Omega), t_k)), \quad (20)$$

where $J(W_k)$ is the Jacobian matrix of the synaptic weight. $\mu > 0$ is the learning rate, computed according to Eq. (21),

$$\mu = \begin{cases} \mu\gamma & \text{if } \Phi(e_{k+1}) > \Phi(e_k), \\ \mu/\gamma & \text{if } \Phi(e_{k+1}) \leq \Phi(e_k), \end{cases} \quad (21)$$

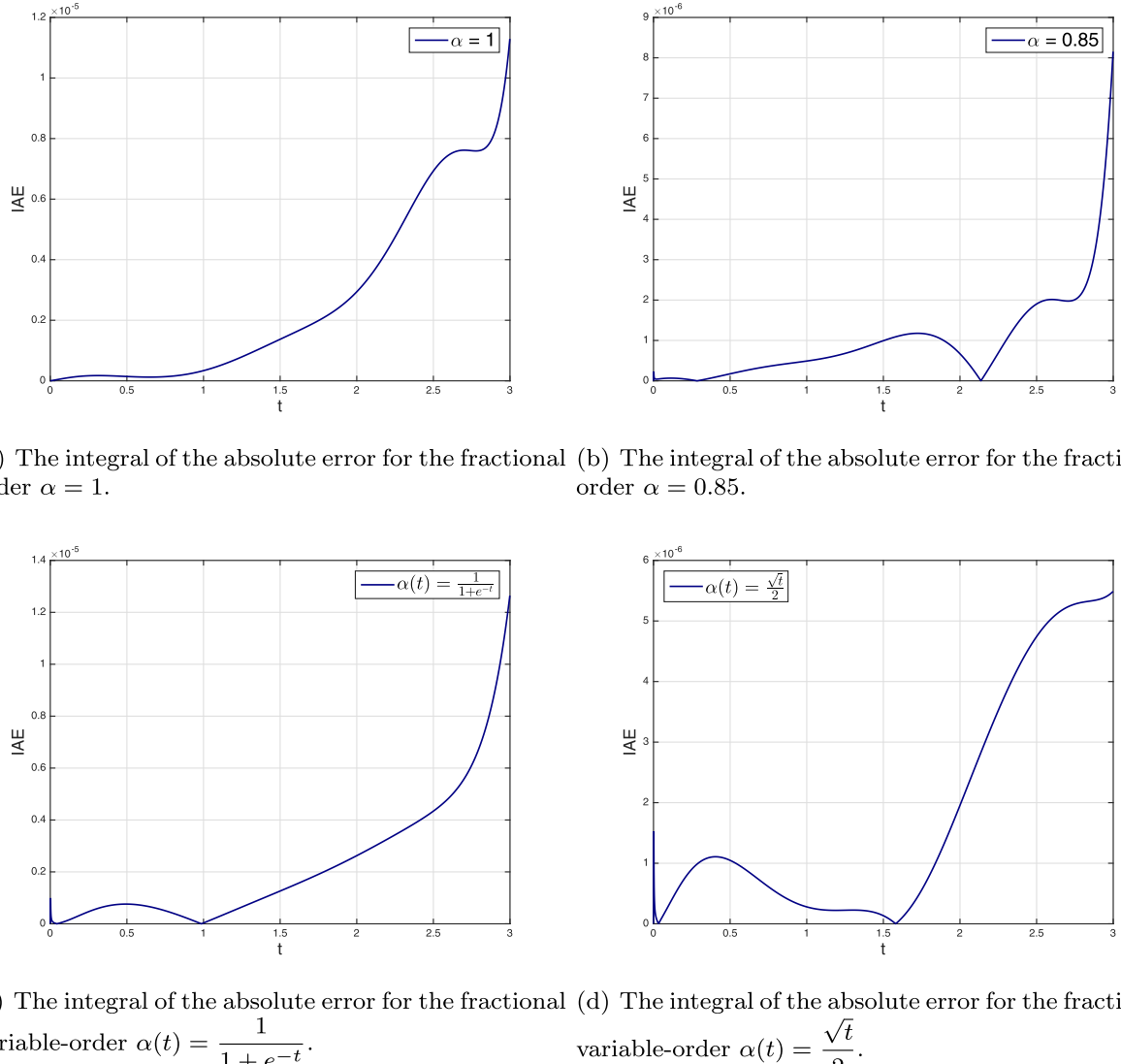
where we can deduce the following: when $\Phi(e)$ decreases through iterations, the parameter μ is divided by a factor γ , when $\Phi(e)$ increases μ is multiplied by γ [60].

4. Results

This section presents a series of examples used to demonstrate that the proposed ANN shown in Eq. (10) allows to obtain the solution of linear FDEs, non-linear FDEs and chaotic systems involving fractional derivatives of the type ABC with variable-order. The ANN used for solving such examples is composed by 5 neurons, i.e., the 2–2–1 ANN shown in Fig. 1. The two neurons in the first layer are used to process for separately the time and output signal, the hidden layer adds degrees of freedom to the neuro-model and the neuron in the output layer adds time signal processing and the output signal. These 2–2–1 ANN is used on all the experiments, as already mentioned the estimation of the $(\kappa_t + \kappa_y + 10)$ synaptic weights was done by the Levenberg–Marquardt algorithm, the software used to develop the experiments was MATLAB 2015a.

Performance of the proposed ANN is quantified by measuring the error norm (see Eq. (22)), measuring the average distance between two points, the FIT (see Eq. (23)), measuring the fit between two signals, the (Integral Absolute Error) IAE (see Eq. (24)) and the (Integral Squared Error) ISE (see Eq. (25))

$$\|e\| = \sqrt{\sum_{i=1}^N e_i^2}, \quad (22)$$

**Fig. 8.** The measured performance indices.

$$FIT = 100 \left(1 - \frac{||\hat{y} - y||}{||y - \bar{y}||} \right), \quad \bar{y} = \frac{1}{N} \sum_{i=1}^N y_i, \quad (23)$$

$$IAE = \sum_{i=1}^N |e_i|, \quad (24)$$

$$ISE = \sum_{i=1}^N e_i^2. \quad (25)$$

Example 1. Consider the following fractional differential equation in Atangana-Baleanu-Caputo sense

$${}_{0}^{ABC}\mathfrak{D}_t^{\alpha(t)}x(t) = -x(t), \quad x(0) = 1, \quad t \in [0, 1]. \quad (26)$$

The analytical solution in the case when $\alpha = 1$ is given by

$$x(t) = E_\alpha(-t^\alpha) = \sum_{i=0}^{\infty} \frac{(-t^\alpha)^i}{\Gamma(\alpha i + 1)}. \quad (27)$$

Considering the Eq. (12), the proposed neural solution is

$$\hat{y}_N = 1 + t\hat{y}(t, \Omega). \quad (28)$$

For validation purposes, the Euler method (Euler) [61], Legendre Operational Matrix (LOM) [62] and the Adams-Basforth-Moulton

method (ABM) [63,64] were developed to show a comparison between the results given by the ANN and different integration methods.

Fig. 2 shows the solution of different integration methods. An enlargement of a part of the figure was made in order to demonstrate that the neural integration with the structure proposed in the Eq. (12) is capable of reaching a similar efficiency compared to other integration methods mentioned before, and to demonstrate that the algorithm of ABM is practically equal to the exact solution of the ANN, therefore, in the remaining simulations the results obtained with the ANN will be compared with the results obtained with the ABM method.

Considering the same example, two more cases are studied: the first one, consists in maintaining the order of the derivative constant in $\alpha = 0.97$; the second case, consists in defining the fractional order α as a variant function over time as $\alpha(t) = \tanh(3 - t)$. The results of the simulations with the ANN are shown in Table 1, synaptic weights and the measured values of the performance indices are also shown, as well as the synaptic weights of the estimated ANNs for the numerical simulations. Fig. 3 shows the approximated solutions obtained with the ABM using the numerical scheme showed in Eq. (9) and the ANN approximation for $\alpha = 0.97$ and $\alpha(t) = \tanh(3 - t)$.

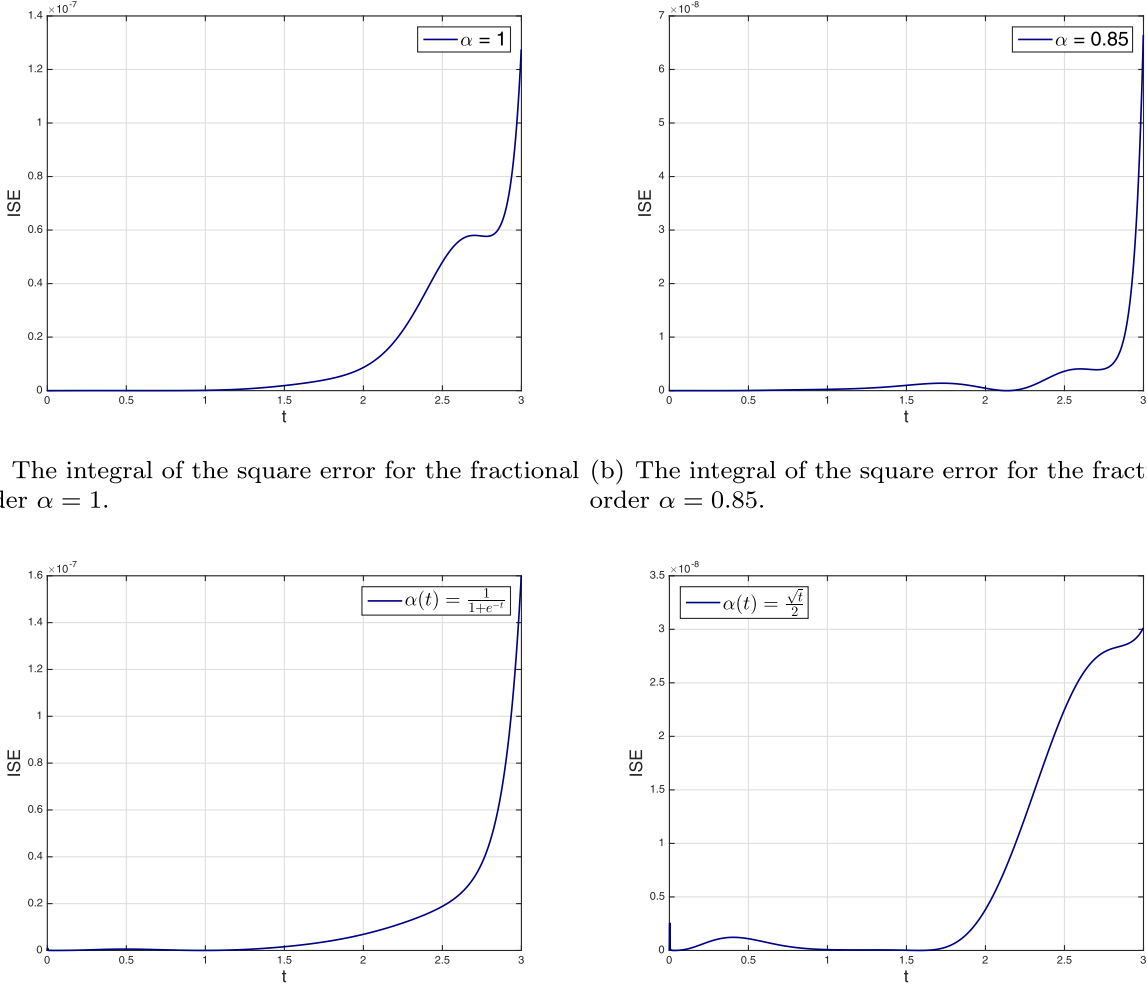


Fig. 9. The measured performance indices.

Table 1
Efficiency and parameters of the ANN.

	$\alpha = 1$	$\alpha = 0.97$	$\alpha(t) = \tanh(3 - t)$
IAE	5.32×10^{-4}	3.01378×10^{-4}	3.03536×10^{-4}
ISE	4.33×10^{-7}	2.50436×10^{-6}	1.6882×10^{-7}
FIT	99.89%	99.74%	99.93%
$\ e\ $	0.020844	0.050043	0.01299
κ_t	7	7	7
$\kappa_{\hat{y}}$	4	4	4
W_g	-1.1813	-4.91115	-3.48598
V_t	-9.0535×10^{-4}	-4.4119×10^{-4}	8.62266×10^{-5}
θ_t	0.3888	0.4819	0.50998
$V_{\hat{y}}$	5.48688	28.3363	16.57773
$\theta_{\hat{y}}$	-0.0940	-0.07184	-0.03627
H_g	0.06079	0.05046	0.047478

For $\alpha = 1$, the estimated synaptic weights are:

$$W_{\hat{y}} = [0.0002 \quad -0.1548 \quad 0.0002 \quad 0.000029]^T,$$

and

$$W_t = [0.4587 \quad 0.0777 \quad -0.4735 \quad 0.6384 \quad 0.6168 \quad -0.8126 \quad 0.6130]^T. \quad (29)$$

For the fractional order $\alpha = 0.97$, the estimated synaptic weights are:

$$W_{\hat{y}} = [0.00000125 \quad -0.00722 \quad 0.0000168 \quad 0.00000287]^T,$$

and

$$W_t = [0.5099 \quad 0.1297 \quad -0.4205 \quad 0.6921 \quad 0.6710 \quad -0.7571 \quad 0.6705]^T. \quad (30)$$

For the fractional variable-order $\alpha(t) = \tanh(3 - t)$, the estimated synaptic weights are:

$$W_{\hat{y}} = [-0.00000213 \quad -0.0173 \quad 0.00000847 \quad 0.00000203]^T,$$

and

$$W_t = [0.4877 \quad 0.1053 \quad -0.4471 \quad 0.6637 \quad 0.6419 \quad -0.7882 \quad 0.6358]^T. \quad (31)$$

Fig. 4 shows the performance indices, IAE (see Eq. (24)) and ISE (see Eq. (25)) for fractional order $\alpha = 0.97$ and $\alpha(t) = \tanh(3 - t)$.

In this example we showed that the neural approximation exhibits a good precision and a fast convergence. In these cases;

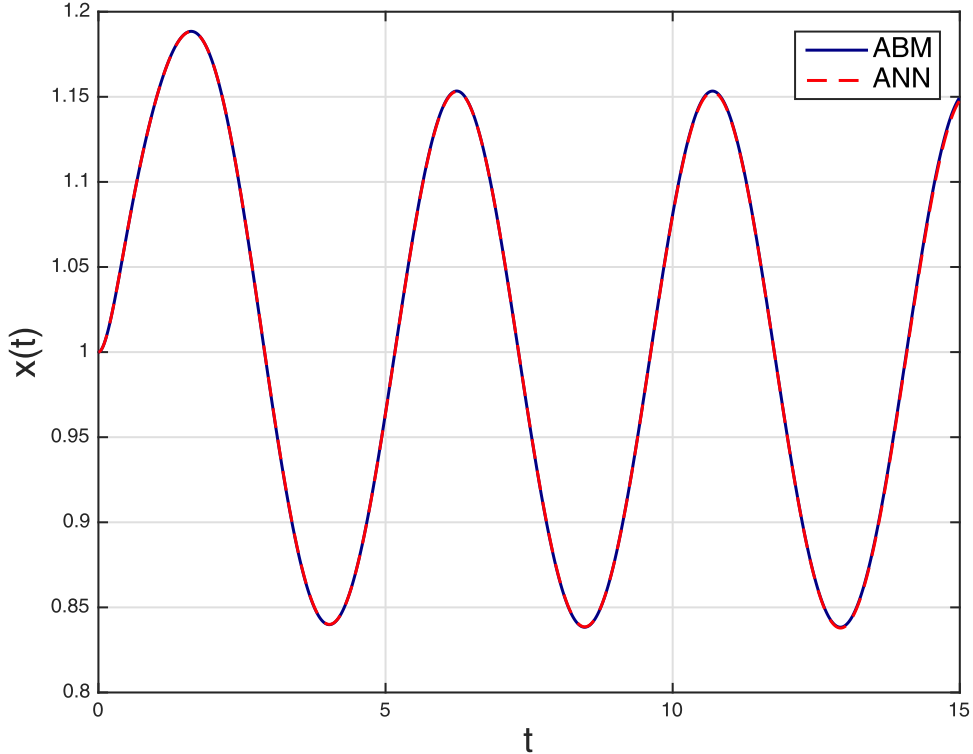


Fig. 10. Numerical solution and the comparison between the ABM and ANN method.

when $\alpha(t) = 1$, the simulation time is 3.48246750 s; for $\alpha(t) = 0.97$, the simulation time is 3.426060535 s and for $\alpha(t) = \tanh(3 - t)$, the simulation time is 3.515249 s. The simulations obtained with the neural structure were compared with the numerical simulations obtained with the application of the numerical scheme showed in Eq. (9). Both simulations showed the same results.

Example 2. Consider the following nonlinear fractional differential equation

$$({}_{t_0}^{ABC}\mathcal{D}_t^{\alpha(t)}x)(t) = g(t) - x^2(t), \quad (32)$$

where

$$\begin{aligned} g(t) = & (2t - 3t^2 + t^3) + \left(2t\left(1 - \alpha + \frac{\alpha t^\alpha}{\Gamma(\alpha + 2)}\right)\right. \\ & \left.- 3t^2\left(1 - \alpha + \frac{2\alpha t^\alpha}{\Gamma(\alpha + 3)}\right) + t^3\left(1 - \alpha + \frac{6\alpha t^\alpha}{\Gamma(\alpha + 4)}\right)\right), \end{aligned} \quad (33)$$

with the initial condition

$$x(0) = 0. \quad (34)$$

The exact solution of the Eq. (32) is given by

$$\begin{aligned} x(t) = & 2t\left(1 - \alpha + \frac{\alpha t^\alpha}{\Gamma(\alpha + 2)}\right) - 3t^2\left(1 - \alpha + \frac{2\alpha t^\alpha}{\Gamma(\alpha + 3)}\right) \\ & + t^3\left(1 - \alpha + \frac{6\alpha t^\alpha}{\Gamma(\alpha + 4)}\right). \end{aligned} \quad (35)$$

Considering the Eq. (12), the neural model is proposed as follows

$$\hat{y}_N = t\hat{y}(t, \Omega). \quad (36)$$

Fig. 5 shows the numerical solution obtained with the neural model given by Eq. (36), and the exact solution given by Eq. (35). Considering the fractional order equal to $\alpha = 0.85$, the Fig. 6 shows the comparison between the neural model and the

Table 2
Efficiency and parameters of the ANN.

	$\alpha = 1$	$\alpha = 0.85$	$\alpha(t) = \frac{1}{1+e^{-t}}$	$\alpha(t) = \frac{\sqrt{t}}{2}$
IAE	79.47×10^{-4}	29.5×10^{-4}	68.73×10^{-4}	54.91×10^{-4}
ISE	4.66×10^{-5}	6.68012×10^{-6}	3.44847×10^{-5}	2.09607×10^{-5}
FIT	99.25%	99.807%	99.46%	99.67%
$\ e\ $	0.2161	0.0819	0.1859	0.1448
K_t	7	7	7	7
K_g	4	4	4	4
W_g	-0.8338	-1.1086	-1.3410	-1.68375
V_t	-3.9013	-5.7714	-8.7902	-12.47788
θ_t	0.0834	0.07481	0.0052	0.05794
V_g	-0.0038	9.3382×10^{-4}	-0.01472	-0.004836
θ_g	0.3687	0.33371	0.4051	0.65873
H_g	0.3268	0.43054	0.060032	0.72639

approximated solutions obtained by the ABM using the numerical scheme showed in Eq. (9). Fig. 7 shows the approximated solutions obtained with the ABM using the numerical scheme showed in Eq. (9) and the ANN approximation for the variable-order $\alpha(t) = \frac{1}{1+e^{-t}}$ and $\alpha(t) = \frac{\sqrt{t}}{2}$ in an interval of $\alpha = \{\alpha : 0 < \alpha \leq 1\}$, $t \in [0, 3]$.

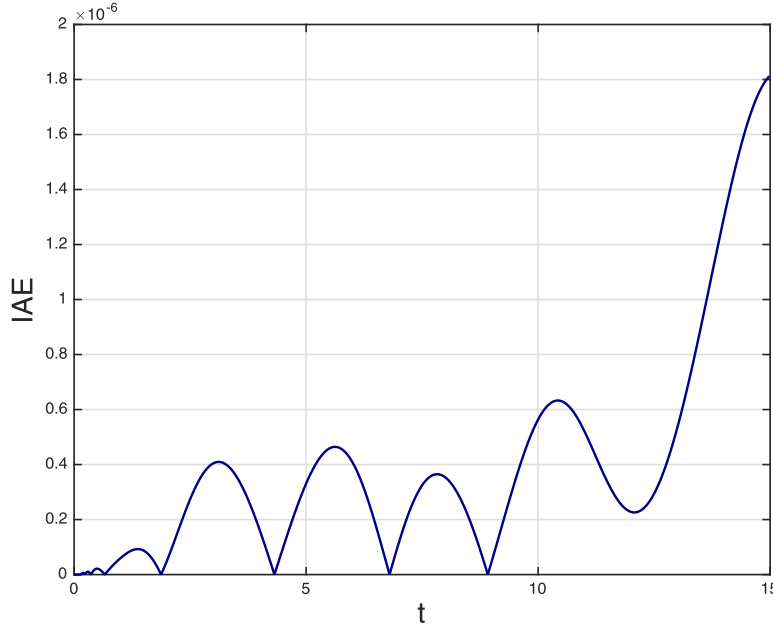
In Figs. 8 and 9 the behavior of the performance indices are shown. In Table 2 some of the results are shown with the purpose of evaluating the efficiency of the proposed ANN and some synaptic weights are shown.

For $\alpha = 1$, the estimated synaptic weights are:

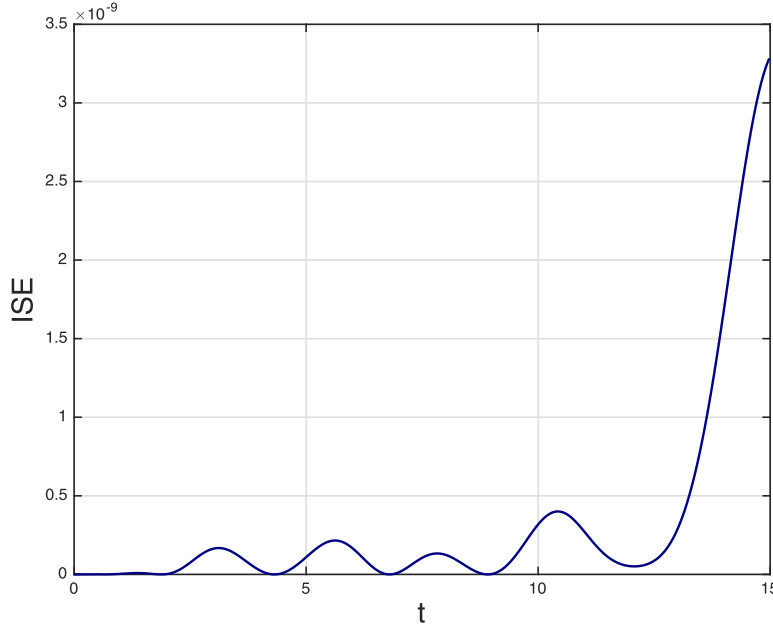
$$W_g = [-0.000055 \quad -0.1124 \quad -0.000488 \quad -0.00088]^T,$$

and

$$W_t = [0.5878 \quad 0.2068 \quad -0.3441 \quad 0.7679 \quad 0.7465 \quad -0.6826 \quad 0.7431]^T. \quad (37)$$



(a) The integral of the absolute error for the fractional variable-order $\alpha(t) = \tanh(t) + 1$.



(b) The integral of the square error for the fractional variable-order $\alpha(t) = \tanh(t) + 1$.

Fig. 11. Numerical solution for $x_1(t)$, $x_2(t)$ and $x_3(t)$.

For the fractional order $\alpha = 0.85$, the estimated synaptic weights are:

$$W_{\hat{y}} = [0.000037 \quad -0.1742 \quad 0.00011 \quad 0.00047]^T,$$

and

$$W_t = [0.4065 \quad 0.0255 \quad -0.5254 \quad 0.5865 \quad 0.5651 \quad -0.8641 \quad 0.5615]^T.$$

(38)

For the fractional variable-order $\alpha(t) = \frac{1}{1+e^{-t}}$, the estimated synaptic weights are:

$$W_{\hat{y}} = [-0.000055 \quad -0.1124 \quad -0.00048 \quad -0.00088]^T,$$

and

$$W_t = [0.5878 \quad 0.2068 \quad -0.3441 \quad 0.7679 \quad 0.7465 \quad -0.6826 \quad 0.7431]^T.$$

(39)

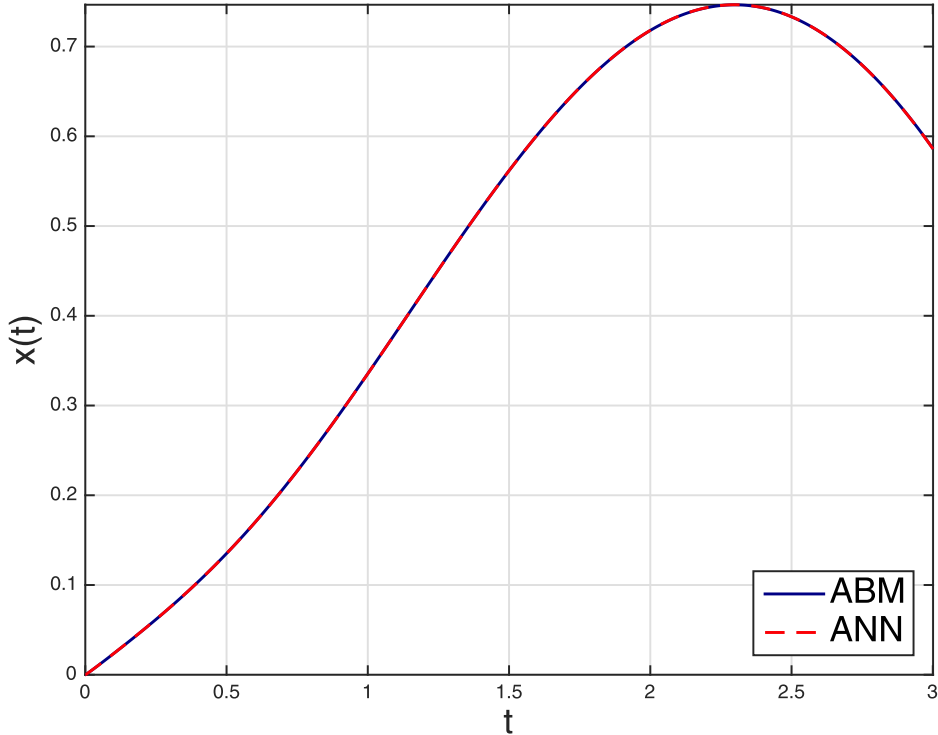


Fig. 12. Numerical solution and the comparison between the ABM and ANN method.

For the fractional variable-order $\alpha(t) = \frac{\sqrt{t}}{2}$, the estimated synaptic weights are:

$$W_y = [-20.8735 \times 10^{-6} \ -0.08010 \ -44.692 \times 10^{-6} \ -000079.066 \times 10^{-6}]^T,$$

and

$$W_t = [0.5026 \ 0.1212 \ -0.4302 \ 0.6811 \ 0.6592 \ -0.7705 \ 0.6545]^T. \quad (40)$$

Example 3. Consider the following fractional differential equation

$$\left({}_{t_0}^{ABC} \mathfrak{D}_t^{\alpha(t)} x \right)(t) = 1 - x(t)^2, \quad x(0) = x'(0) = 1 \quad \text{and} \quad \alpha(t) = \tanh(t) + 1. \quad (41)$$

Considering the fractional order $\alpha(t) = \{\alpha : 1 < \alpha \leq 2\}$, where, $[\alpha(t)] = 2$. According to the Eq. (12), the neuro-solution is given by

$$\hat{y}_N = 1 + t + t^2 \hat{y}(t, \Omega). \quad (42)$$

The results of the simulations with the ANN and ABM are shown in Fig. 10. The performance indices are shown in Fig. 11. For this figure, in a) the IAE is shown, where it can be appreciated that in time equal to zero this performance index is null, and in b) is shown the ISE. Table 3 shows synaptic weights and the measured values of the performance indices.

For the fractional variable-order $\alpha(t) = \tanh(t) + 1$, the estimated synaptic weights are:

$$W_y = [0.42 \ -0.21 \ -0.05 \ -0.18 \ 0.07 \ 0.01 \ 0.009]^T$$

Table 3
Efficiency of the ANN compared with the ABM method.

	$\alpha(t) = \tanh(t) + 1$
IAE	6.0039×10^{-4}
ISE	4.7668×10^{-7}
FIT	99.94%
$\ e\ $	0.0218
K_t	15
K_g	15
W_g	14.2782
V_t	8.2115
θ_t	0.0114
V_y	2.006
θ_y	1.8333
H_g	-2.0061

and

$$W_t = [44.65 \ -33.10 \ -10.11 \ 5.91 \ 17.17 \ 3.42 \ -0.46 \ 11.67 \ -4.2 \ -7.4 \ \dots \ 1.73 \ -0.71 \ -2.59 \ 0.78 \ -20.74]^T. \quad (43)$$

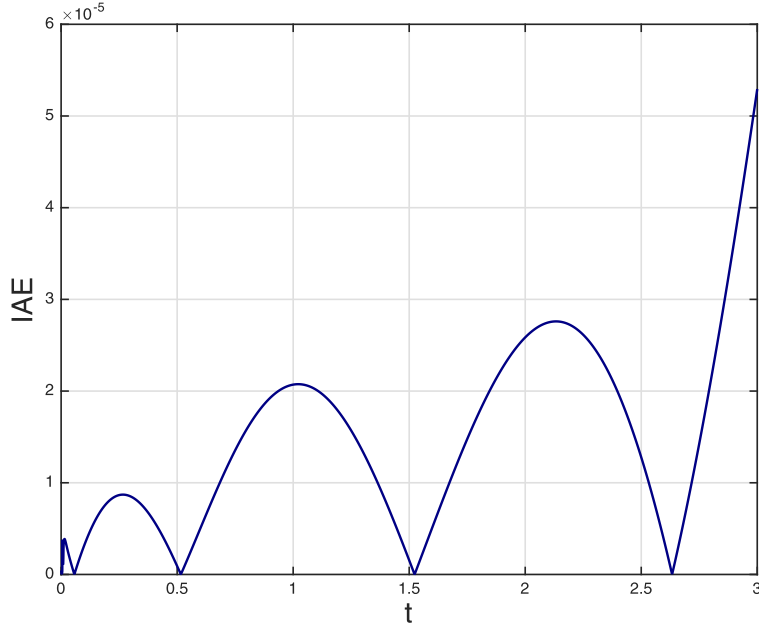
Example 4. Consider the following fractional differential equation

$$\left({}_{t_0}^{ABC} \mathfrak{D}_t^{\alpha(t)} x \right)(t) = \sin(t) - x(t), \quad x(0) = x'(0) = 0. \quad (44)$$

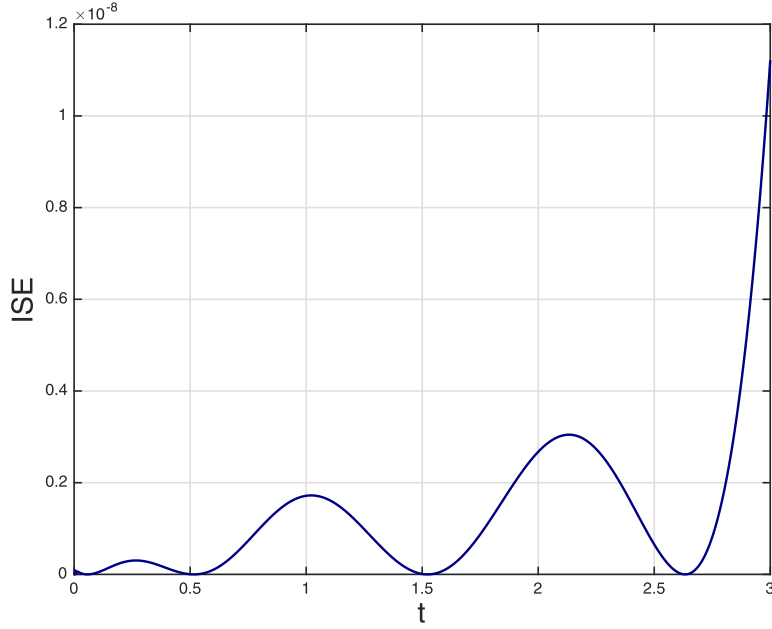
The exact solution of the Eq. (44) is given by

$$x(t) = \frac{1}{2} e^{-t} + \frac{1}{2} \sin(t) - \frac{1}{2} \cos(t). \quad (45)$$

In this example two cases are studied: in the first one the fractional order is considered as $\alpha(t) \in [0, 1]$, where, $\alpha(t) = \tanh(t + 1)$; the second case consists in defining the fractional order α as a variant function over the interval $\alpha(t) \in [1, 2]$, where, $\alpha(t) = \tanh(t) + 1$.



(a) The integral of the absolute error for the fractional variable-order $\alpha(t) = \tanh(t + 1)$.



(b) The integral of the square error for the fractional variable-order $\alpha(t) = \tanh(t + 1)$.

Fig. 13. Numerical solution for $x_1(t)$, $x_2(t)$ and $x_3(t)$.

Case 1. Considering the Eq. (12), the neural model is proposed as

$$\hat{y}_N = t\hat{y}(t, \Omega). \quad (46)$$

The results of the simulations with the ANN and ABM are shown in Fig. 12. The performance indices are shown in Fig. 13. For this figure, in a)-b) are showed the integral of the absolute error and the integral of the squared error. In both figures it can be

seen that the performance indices are small. Table 4 shows synaptic weights and the measured values of the performance indices.

For the fractional variable-order $\alpha(t) = \tanh(t + 1)$, the estimated synaptic weights are:

$$W_{\hat{y}} = [-0.286 \quad 0.631 \quad -0.242 \quad -0.048 \quad 0.0129]^T,$$

and

$$W_t = [-0.098 \quad -1.919 \quad 5.554 \quad -4.962 \quad 1.425]^T. \quad (47)$$

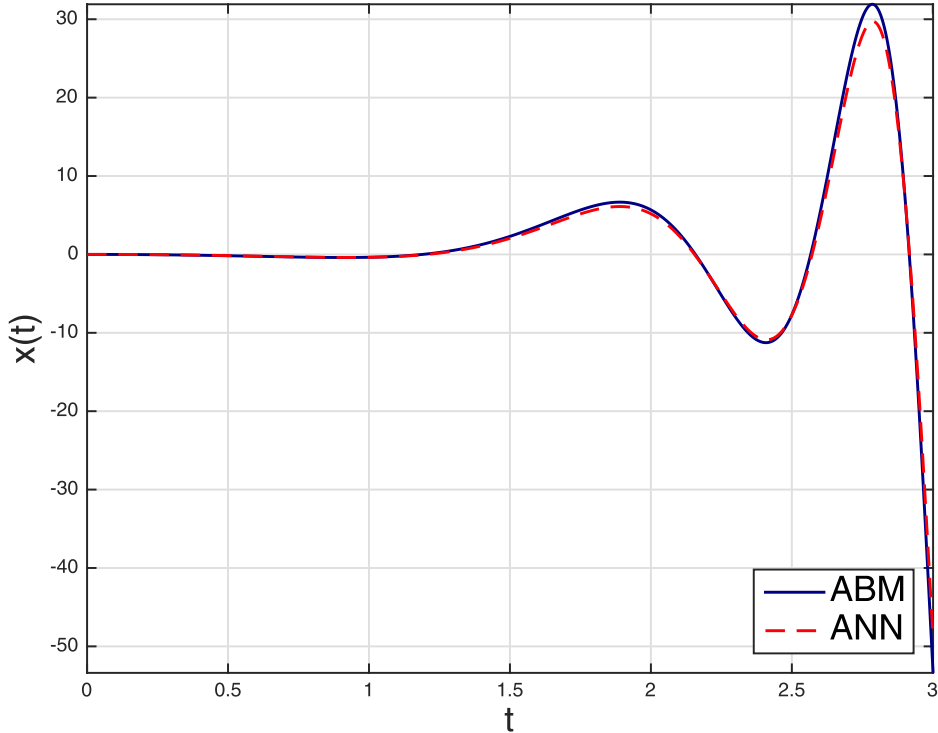


Fig. 14. Numerical solution and the comparison between the ABM and ANN method.

Table 4
Efficiency of the ANN compared with the ABM method.

$\alpha(t) = \tanh(t + 1)$	
IAE	0.0447
ISE	3.8942×10^{-6}
FIT	99.98%
$\ e\ $	0.0039
K_t	5
K_y	5
W_g	-7.8511
V_t	15.0154
θ_t	-0.0583
V_y	-488
θ_y	0.0474
H_g	24

Table 5
Efficiency of the ANN compared with the ABM method.

$\alpha(t) = \tanh(t + 1)$	
IAE	296
ISE	431
FIT	92.20%
$\ e\ $	41.67
K_t	5
K_y	5
W_g	143
V_t	339874
θ_t	-3.79
V_y	-2066176
θ_y	-3.01
H_g	-1726643

Case 2. Considering the Eq. (12), where, $\lceil \alpha(t) \rceil = 2$, the neural model proposed is

$$\hat{y}_N = t + t^2 \hat{y}(t, \Omega). \quad (48)$$

The results of the simulations of the Eq. (48) with the ANN and ABM for a variable-order between $1 < \alpha(t) \leq 2$ are shown in Fig. 14. The performance indices are shown in Fig. 15. For this figure, in a-b) are showed the integral of the absolute error and the integral of the squared error. In both figures it can be seen an increase in the amplitude of the performance indices, due to the rapid dynamics of the system. Table 5 shows synaptic weights and the measured values of the performance indices.

For the fractional variable-order $\alpha(t) = \tanh(t + 1)$, the estimated synaptic weights are:

$$W_{\hat{y}} = [-0.00014 \quad 0.0015]^T,$$

and

$$W_t = [-206.46 \quad -57.67]^T. \quad (49)$$

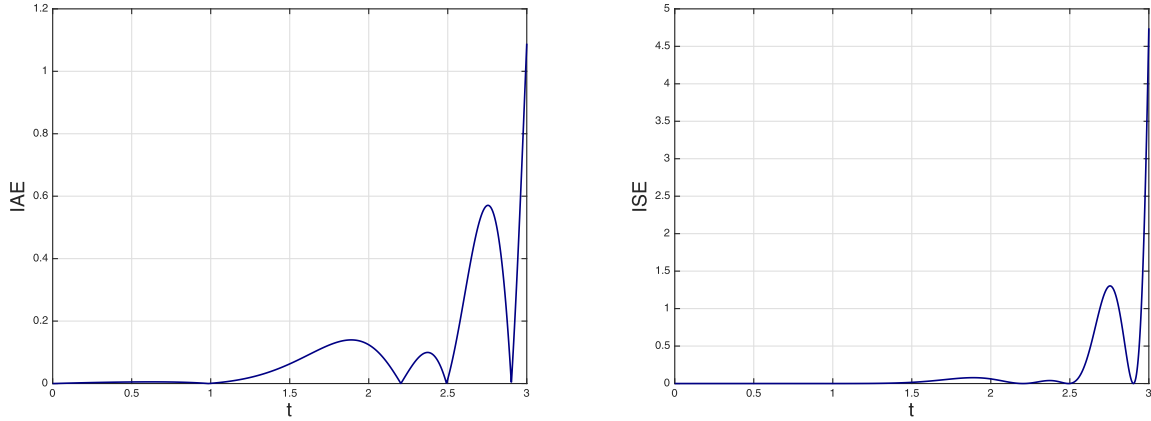
Example 5. In this example the Willamowski–Rössler oscillator was considered. The system is described by the following Eqs.

$$\begin{aligned} {}^{(ABC)}\mathcal{D}_t^{\alpha(t)}x_1(t) &= -(x_3(t) + x_2(t)), \\ {}^{(ABC)}\mathcal{D}_t^{\alpha(t)}x_2(t) &= x_1(t) + \varepsilon_1 x_2(t), \\ {}^{(ABC)}\mathcal{D}_t^{\alpha(t)}x_3(t) &= \varepsilon_2 + x_3(t)(x_1(t) - \varepsilon_3), \end{aligned} \quad (50)$$

where $\varepsilon_1 = 0.1$, $\varepsilon_2 = 0.1$, $\varepsilon_3 = 14$, $x_1(0) = 4.87623$, $x_2(0) = 4.87623$ and $x_3(0) = 0.1278$. For this example, we consider a fractional variable-order $\alpha(t) = \tanh(t + 1)$. Considering the Eq. (12), we proposed three neuro-solutions for each fractional differential equation, these solutions are given by

$$\begin{aligned} \hat{y}_{N1} &= 4.87623 + t \hat{y}(t, \Omega_1), \\ \hat{y}_{N2} &= 4.87623 + t \hat{y}(t, \Omega_2), \\ \hat{y}_{N3} &= 0.12799 + t \hat{y}(t, \Omega_3). \end{aligned} \quad (51)$$

The numerical solutions obtained with the neuro-structure described in the Eq. (51) are compared with the simulations obtained via the application of the ABM method showed in the Eq. (9). Fig. 16 shows the behavior of the three states $x_1(t)$, $x_2(t)$ and



(a) The integral of the absolute error for the fractional variable-order $\alpha(t) = \tanh(t) + 1$.
(b) The integral of the square error for the fractional variable-order $\alpha(t) = \tanh(t) + 1$.

Fig. 15. Numerical solution for $x_1(t)$, $x_2(t)$ and $x_3(t)$.

Table 6
Efficiency of the ANN compared with the ABM method.

	$x_1(t)$	$x_2(t)$	$x_3(t)$
IAE	77.6805	61.6614	21.8081
ISE	17.6534	11.0497	18.2837
FIT	98.3441	98.6572	95.795
$\ \epsilon\ $	42.016	33.2411	42.7595
K_t	7	7	5
K_g	7	7	5
W_g	1.56223	1.4371	1.5791
V_t	16.8104	15.4640	11.0145
θ_t	0.1430	-0.0076	-0.0505
V_g	-0.0203	-0.0187	0.00316
θ_g	2.6345	2.5115	0.2728
H_g	-2.3677	0.1645	0.5531

$x_3(t)$. In Fig. 17a) it is shown the phase diagram obtained through the integration of each state ($x_1(t)$, $x_2(t)$ and $x_3(t)$) considering the ABM method showed in 9. In Fig. 17b) it is shown the phase diagram obtained through the estimation with the proposed neural network described in Eq. (51). Finally, the Fig. 18 shows the behavior of the performance indices. To summarize, the neuro-structure was implemented in order to obtain a neural solution of the Willamowski-Rössler oscillator. The values of the performance indices over 500 seconds and the neural network parameters are shown in Table 6.

For $x_1(t)$, the estimated synaptic weights are:

$$W_{\hat{y}} = \begin{bmatrix} -80.58 \times 10^{-9} & 0.06006 & 0.00055 & 0.00006515 \\ -7.60 \times 10^{-6} & 0.000153 & -0.000579 \end{bmatrix}^T,$$

and

$$W_t = [0.6233 \ 0.6009 \ -0.8293 \ 0.5952 \ 0.3506 \ 0.0170 \ 1.1825]^T. \quad (52)$$

For $x_2(t)$, the estimated synaptic weights are:

$$W_{\hat{y}} = \begin{bmatrix} 370.36 \times 10^{-10} & -0.0405 & -0.0005 & 0.0001 & 0.00004 \\ -0.00019 & 0.0004 \end{bmatrix}^T,$$

and

$$W_t = [0.6097 \ 0.5885 \ -0.8403 \ 0.5856 \ 0.3422 \ 0.0097 \ 1.1761]^T. \quad (53)$$

For $x_3(t)$, the estimated synaptic weights are:

$$W_{\hat{y}} = [2.74 \times 10^{-9} \ 0.0906 \ 0.0005 \ -0.0001 \ -0.00014]^T,$$

and

$$W_t = [-96.57 \ -7.2719 \ 79.4373 \ 22.681 \ 20.9501]^T. \quad (54)$$

Example 6. In this example we consider a chaos generator (2D-grid scroll) [65], the fractional Eqs. are given by

$$\left({}_{t_0}^{ABC} \mathcal{D}_t^{\alpha(t)} \mathbf{x} \right)(t) = \mathbf{A}\mathbf{x}(t) + \mathbf{B}\Psi(\mathbf{x}, t), \quad (55)$$

where

$$\mathbf{A} = \begin{bmatrix} 0 & 1 & 0 \\ 0 & 0 & 1 \\ -a & -a & -a \end{bmatrix}, \quad \mathbf{B} = \begin{bmatrix} -1 & 0 & 0 \\ 0 & 0 & 0 \\ 0 & 0 & a \end{bmatrix},$$

$$\Psi(\mathbf{x}, t) = \begin{bmatrix} f_1(x_2) \\ 0 \\ f_2(x_1) \end{bmatrix}, \quad (56)$$

with

$$f_1(x_2) = \sum_{i=1}^{M_{x_2}} G_{\frac{1-2i}{2}}(x_2) + \sum_{i=1}^{N_{x_2}} G_{\frac{2i-1}{2}}(x_2),$$

$$f_2(x_1) = \sum_{i=1}^{m-1} \gamma G_{\zeta}(x_1), \quad (57)$$

where

$$\zeta = M_{x_2} + 0.5 + (i-1)(M_{x_2} + N_{x_2} + 1),$$

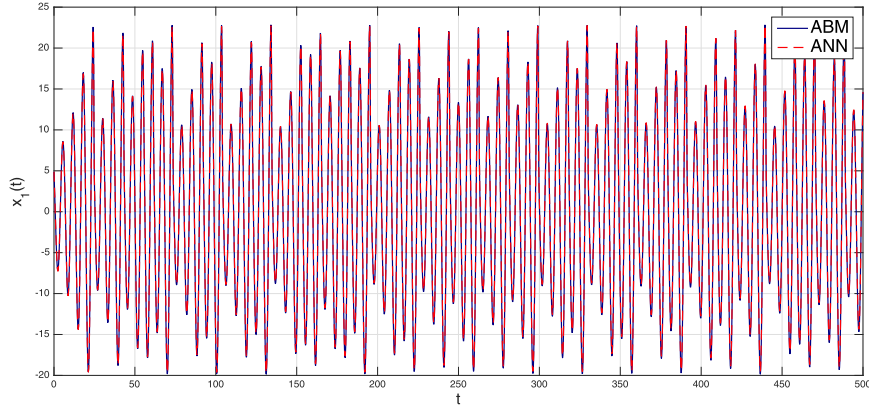
$$\gamma = M_{x_2} + N_{x_2} + 1, \text{ with}$$

$$g_{\zeta}(x_i) = \begin{cases} 1, & x_i \geq \zeta \quad \zeta > 0, \\ 0, & x_i < \zeta \quad \zeta > 0, \\ 0, & x_i \leq \zeta \quad \zeta < 0, \\ -1, & x_i < \zeta \quad \zeta < 0. \end{cases} \quad (58)$$

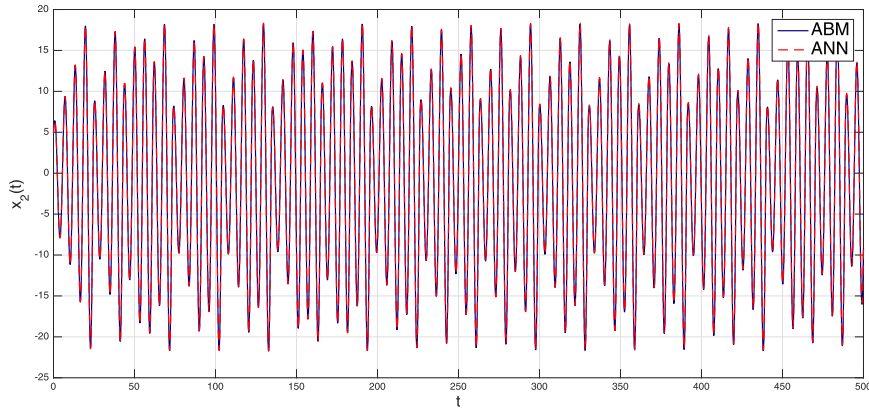
For this example, we consider $M_{x_2} = 0$, $N_{x_2} = 1$, $m = 2$, $f_1(x_2) = G_{0.5}(x_2)$, $f_2(x_1) = 2G_{0.5}(x_1)$, $a = 0.3$ and fractional order $\alpha(t) = \tanh(t+1)$. Considering the Eq. (12), the neuro-model for this example is given by

$$\begin{aligned} \hat{y}_{N1} &= 0.8193 + t\hat{y}(t, \Omega_1), \\ \hat{y}_{N2} &= 1.0216 + t\hat{y}(t, \Omega_2), \\ \hat{y}_{N3} &= 0.0238 + t\hat{y}(t, \Omega_3), \end{aligned} \quad (59)$$

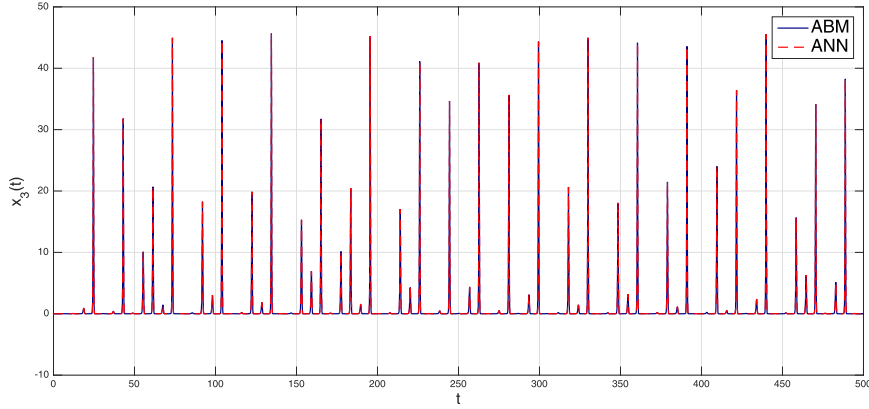
Fig. 19 shows the approximated numerical simulations of the Eq. (55). In (a)-(b)-(c) the states ($x_1(t)$, $x_2(t)$ and $x_3(t)$) obtained



(a) Approximated solution with the ABM and ANN method for $x_1(t)$ and fractional variable-order $\alpha(t) = \tanh(t + 1)$.



(b) Approximated solution with the ABM and ANN method for $x_2(t)$ and fractional variable-order $\alpha(t) = \tanh(t + 1)$.



(c) Approximated solution with the ABM and ANN method for $x_3(t)$ and fractional variable-order $\alpha(t) = \tanh(t + 1)$.

Fig. 16. Numerical solution for $x_1(t)$, $x_2(t)$ and $x_3(t)$.

with ABM method, Eq. (9), and the obtained with the neuro-structure Eq. (59) are shown.

Fig. 20 describes the performance indices for each state ($x_1(t)$, $x_2(t)$ and $x_3(t)$). This figure shows that the performance indices are relatively small and are equal to zero when $t = 0$.

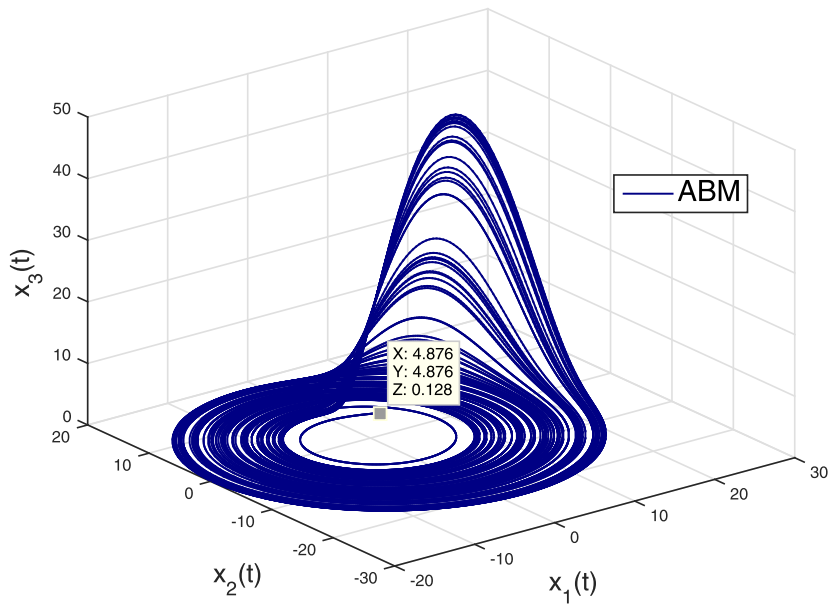
In Fig. 21 the phase diagrams are shown. The first one correspond to the behavior of the states through the implementation of the ABM method, and for the second case, we present the phase diagram obtained by the neural states shown in Eq. (59).

For $x_1(t)$, the estimated synaptic weights are:

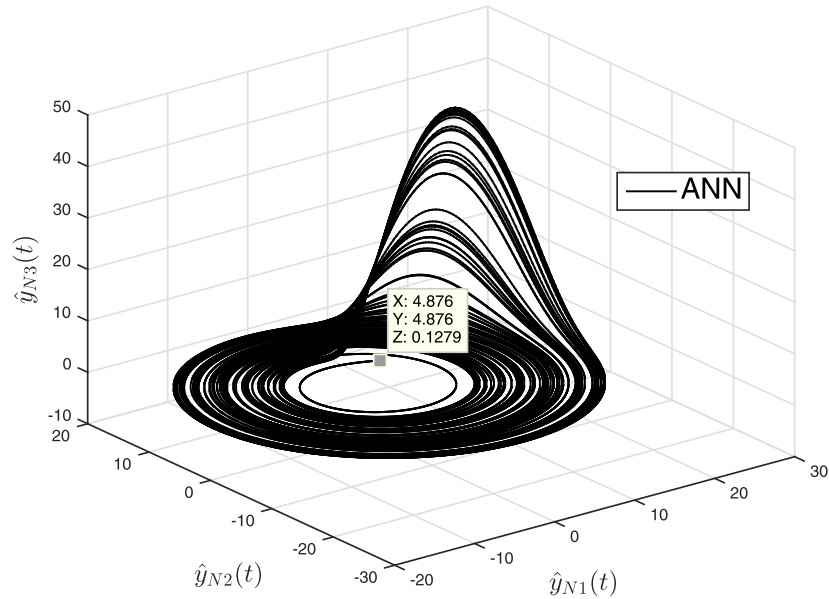
$$W_{\hat{y}} = \begin{bmatrix} 0.7712 & -0.0010 & -5.95 \times 10^{-5} & -12.012 \times 10^{-6} \\ -7.147 \times 10^{-6} & -38.50 \times 10^{-6} & -0.0018 \end{bmatrix}^T,$$

and

$$W_t = [0.588 \ 0.567 \ -0.860 \ 0.565 \ 0.322 \ -0.009 \ 1.157]^T. \quad (60)$$



(a) Phase diagram for the three states of the Willamowski-Rössler oscillator, Eq. (50) obtained by the ABM algorithm.



(b) Phase diagram for the three states of the Willamowski-Rössler oscillator, Eq. (51) obtained for the neuro-structure proposed.

Fig. 17. Phase diagram for the Willamowski-Rössler oscillator, Eq. (51). In (a) the simulation obtained with the neuro-structure; in (b) the numerical simulation obtained with the application of the ABM method.

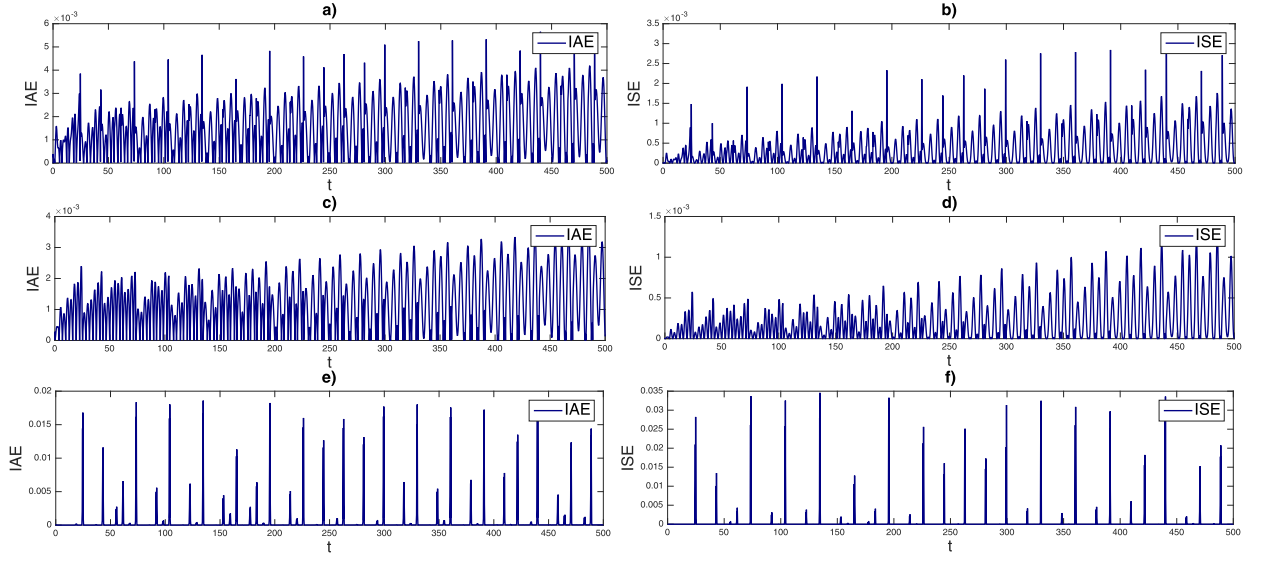
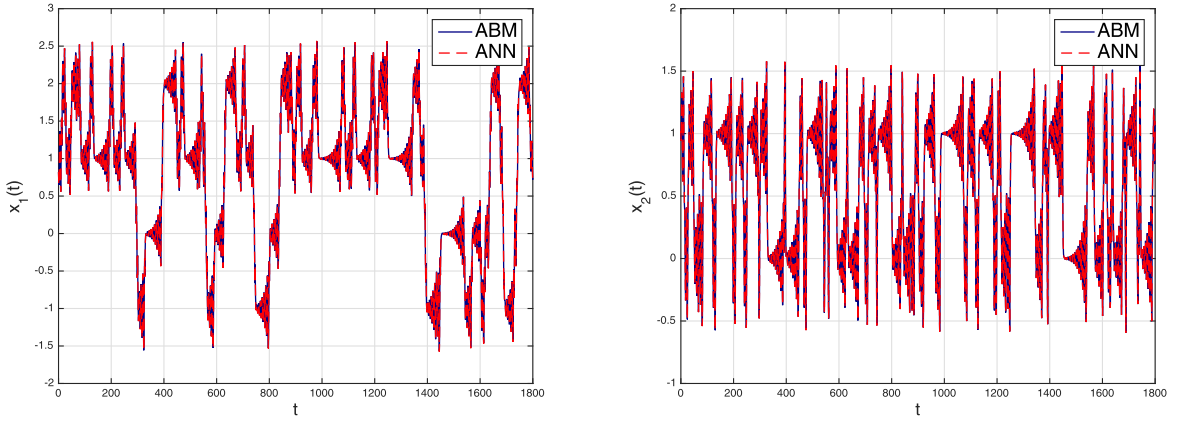
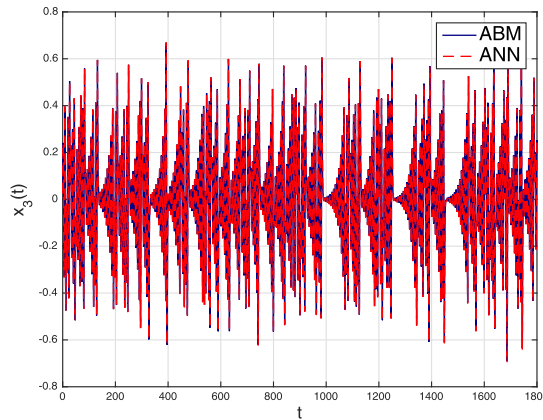


Fig. 18. Performance indices. In a)-b) the integral of the absolute error and square error respectively for the state $x_1(t)$. In c)-d) the integral of the absolute error and square error respectively for the state $x_2(t)$. In e)-f) the integral of the absolute error and square error respectively for the state $x_3(t)$.

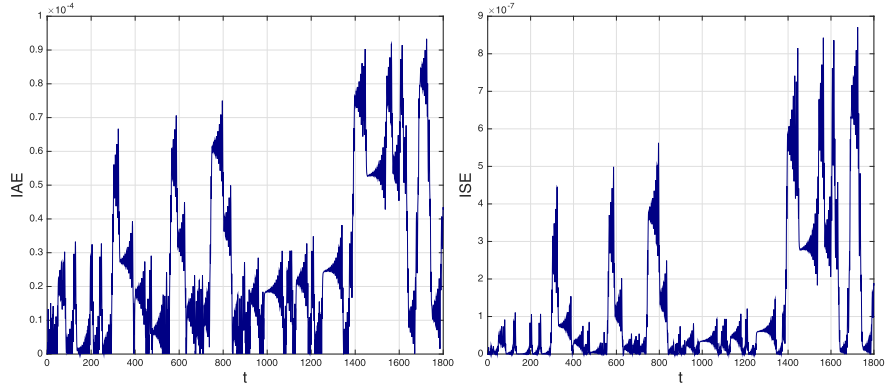


(a) Approximated solution with the ABM (blue) and (b) Approximated solution with the ABM (blue) and
ANN (red) method for the state $x_1(t)$. (c) Approximated solution with the ABM (blue) and
ANN (red) method for the state $x_2(t)$.

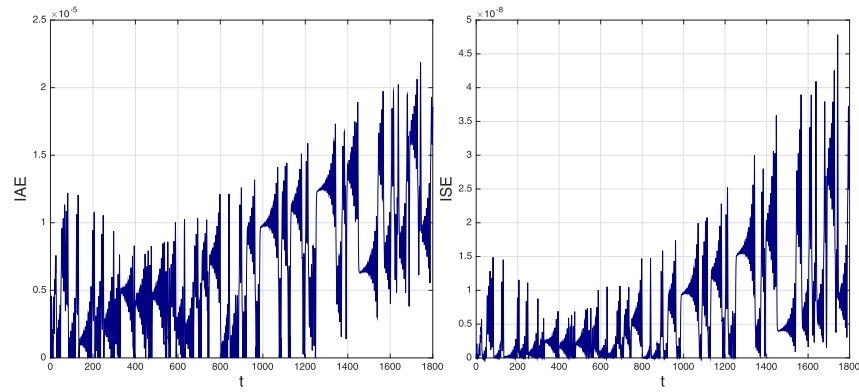


(c) Approximated solution with the ABM (blue) and
ANN (red) method for the state $x_3(t)$.

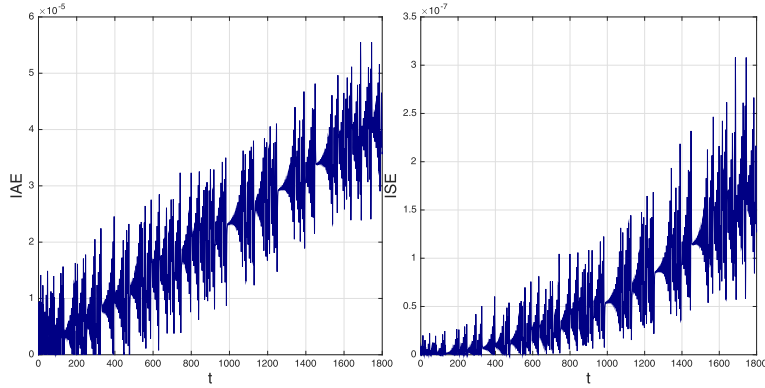
Fig. 19. Numerical solution obtained with the application of the ABM and the ANN scheme for the 2D-grid scroll.



(a) The integral of the absolute error (left) and the integral of the square error (right) for the state $x_1(t)$.



(b) The integral of the absolute error (left) and the integral of the square error (right) for the state $x_2(t)$.



(c) The integral of the absolute error (left) and the integral of the square error (right) for the state $x_3(t)$.

Fig. 20. The measured performance indices from the 2D-grid scroll.

For $x_2(t)$, the estimated synaptic weights are:

$$W_{\hat{y}} = [-0.7357 \quad 0.0008 \quad 0.0003 \quad 0.0001 \quad 0.00004 \quad 0.00002 \quad -0.0004]^T,$$

and

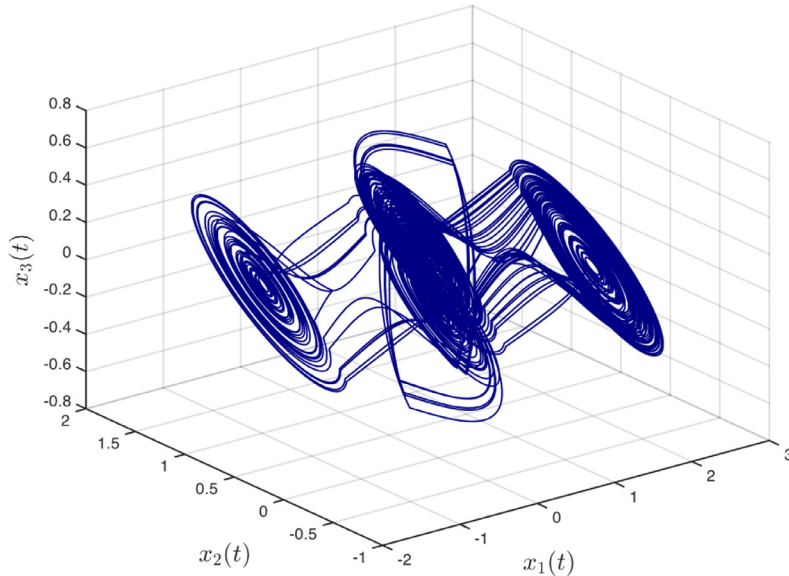
$$W_t = [0.586 \quad 0.565 \quad -0.862 \quad 0.564 \quad 0.322 \quad -0.009 \quad 1.157]^T. \quad (61)$$

For $x_3(t)$, the estimated synaptic weights are:

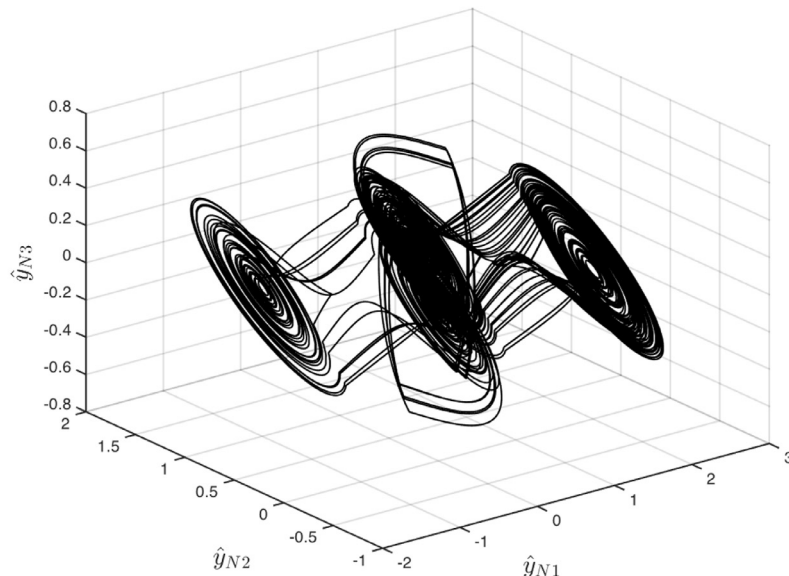
$$W_{\hat{y}} = \begin{bmatrix} 0.7713 & -0.001 & -0.00005 & -0.00001 & -0.000007 \\ -0.00003 & -0.0018 \end{bmatrix}^T, \quad (62)$$

and

$$W_t = [0.588 \quad 0.567 \quad -0.860 \quad 0.565 \quad 0.322 \quad -0.009 \quad 1.157]^T. \quad (63)$$



(a) Phase diagram for the three states of the 2D-grid scroll obtained by the ABM algorithm.



(b) Phase diagram for the three states of the 2D-grid scroll obtained by the neuro-structure proposed.

Fig. 21. Phase diagram for the 2D-grid scroll comparison between ABM and ANN schemes.

The values of the performance indices and the neural network parameters are shown in [Table 7](#).

5. Conclusions

In this paper, a neural network structure was proposed for the integration of fractional differential equations of variable-order with Mittag-Leffler kernel in Liouville–Caputo sense. The effectiveness and applicability of this approach were validated by solving different types of FDEs, the Willamowski–Rössler oscillator and a

chaos generator (2D-grid scroll). We obtain both a good precision and a fast convergence of the proposed technique for the examples considered. The neural network architecture proposed in this work showed the capability to achieve the approximate solutions of the examples studied. For the estimating of the unknown synaptic weights, the Levenberg–Marquardt algorithm showed efficient results. The comparison between the numerical results obtained by the analytical solutions and the approximate numerical solutions based on ANN showed the powerfulness and reliability of the

Table 7

Efficiency of the ANN compared to the ABM and parameters for the 2D-grid scroll.

	$x_1(t)$	$x_2(t)$	$x_3(t)$
IAE	4.7521	1.2373	3.8553
ISE	0.0219	0.0012	0.01102
FIT	99.7287	99.8913	98.8644
$\ e\ $	1.4828	0.3515	1.0498
K_t	7	7	7
K_y	7	7	7
W_g	-0.6116	0.7704	-0.6112
V_t	1.3056	-1.3619	1.3053
θ_t	0.0239	-0.0070	0.0239
V_y	-0.0053	0.1589	-0.0053
θ_y	2.4603	2.4580	2.4603
H_g	-0.0258	-0.1685	-0.0258

neuro-structure proposed. The computer used for obtaining the results in this paper is an Intel Core i7, 2.6 GHz processor, 16.0-GB RAM (Matlab R.2013a).

Competing interests

The authors declare that there is no conflict of interests regarding the publication of this paper.

Authors' contributions

All authors contributed equally and significantly in writing this article. All authors read and approved the final manuscript.

Acknowledgments

Carlos Zúñiga Aguilar acknowledges the support provided by CONACyT through the assignment doctoral fellowship. José Francisco Gómez Aguilar acknowledges the support provided by CONACyT: Cátedras CONACyT para jóvenes investigadores 2014.

References

- [1] Mainardi F. An historical perspective on fractional calculus in linear viscoelasticity. *Fract Calculus Appl Anal* 2012;15(4):712–17.
- [2] Mishra V, Vishal K, Das S, Ong SH. On the solution of the nonlinear fractional diffusion-wave equation with absorption: a homotopy approach. *Zeitschrift für Naturforschung A* 2014;69(3–4):135–44.
- [3] Morales-Delgado VF, Taneco-Hernández MA, Gómez-Aguilar JF. On the solutions of fractional order of evolution equations. *Eur Phys J Plus* 2017;132(1):47.
- [4] Ouannas A, Al-Sawalha MM, Ziar T. Fractional chaos synchronization schemes for different dimensional systems with non-identical fractional-orders via two scaling matrices. *Optik-Int J Light Electron Opt* 2016;127(20):8410–18.
- [5] Kumar S, Kumar A, Argyros IK. A new analysis for the keller-segel model of fractional order. *Numer Algorithms* 2017a;75(1):213–28.
- [6] Kumar D, Singh J, Baleanu D. A hybrid computational approach for klein-gordon equations on cantor sets. *Nonlinear Dyn* 2017b;87(1):511–17.
- [7] Kumar S. A new analytical modelling for fractional telegraph equation via laplace transform. *Appl Math Model* 2014;38(13):3154–63.
- [8] Zaman SF, Baleanu D, Petráš I. Measurement of para-xylene diffusivity in zeolites and analyzing desorption curves using the mittag-leffler function. *Fract Calculus Appl Anal* 2016;19(2):551–60.
- [9] Ma HC, Yao DD, Peng XF. Exact solutions of non-linear fractional partial differential equations by fractional sub-equation method. *Thermal Science* 2015;19(4):1239–44.
- [10] Mohyud-Din ST, Nawaz T, Azhar E, Akbar MA. Fractional sub-equation method to space-time fractional calogero-degasperis and potential kadomtsev-petviashvili equations. *J Taibah Univ Sci* 2015;1–6.
- [11] Feng D, Li K. Exact traveling wave solutions for a generalized hirota-satsuma coupled kdv equation by fan sub-equation method. *Phys Lett A* 2011;375(23):2201–10.
- [12] Zhang Y, Cattani C, Yang XJ. Local fractional homotopy perturbation method for solving non-homogeneous heat conduction equations in fractal domains. *Entropy* 2015;17(10):6753–64.
- [13] Singh J, Gupta PK, Rai KN. Homotopy perturbation method to space-time fractional solidification in a finite slab. *Appl Math Model* 2011;35(4):1937–45.
- [14] Kushwaha MS. Homotopy perturbation method for a limit case stefan problem governed by fractional diffusion equation. *Appl Math Model* 2013;37(5):3589–99.
- [15] Das N, Singh R, Wazwaz AM, Kumar J. An algorithm based on the variational iteration technique for the bratu-type and the lane-emden problems. *J Math Chem* 2016;54(2):527–51.
- [16] Hao YJ, Yang AM. The local fractional iteration solution for the diffusion problem in fractal media. *Thermal Sci* 2016;20(3):S743–6.
- [17] Khader MM, Adel M. Analytical and numerical validation for solving the fractional klein-gordon equation using the fractional complex transform and variational iteration methods. *Nonlinear Eng* 2016;5(3):141–5.
- [18] Turkyilmazoglu M. Convergent optimal variational iteration method and applications to heat and fluid flow problems. *Int J Numer Methods Heat Fluid Flow* 2016;26(3/4):790–804.
- [19] Kumar D, Singh J, Kumar S. Analytic and approximate solutions of space-time fractional telegraph equations via laplace transform. *Walailak J Sci Technol (WJST)* 2013;11(8):711–28.
- [20] Irandoust-Pakchin S, Javidi M, Kheiri H. Analytical solutions for the fractional nonlinear cable equation using a modified homotopy perturbation and separation of variables methods. *Comput Math Math Phys* 2016;56(1):116–31.
- [21] Kumar D, Singh J, Kumar S. Numerical computation of nonlinear fractional zakharov-kuznetsov equation arising in ion-acoustic waves. *J Egyptian Math Soc* 2014;22(3):373–8.
- [22] Xu Y, Sun K, He S, Zhang L. Dynamics of a fractional-order simplified unified system based on the adomian decomposition method. *Eur Phys J Plus* 2016;131(6):1–12.
- [23] Wang HH, Sun KH, He SB. Dynamic analysis and implementation of a digital signal processor of a fractional-order lorenz-stenflo system based on the adomian decomposition method. *Phys Scr* 2014;90(1):015206.
- [24] Khodabakhshi N, Mansour Vaezpour S, Baleanu D. Numerical solutions of the initial value problem for fractional differential equations by modification of the adomian decomposition method. *Fract Calculus Appl Anal* 2014;17(2):382–400.
- [25] Ray SS, Gupta AK. Numerical solution of fractional partial differential equation of parabolic type with dirichlet boundary conditions using two-dimensional legendre wavelets method. *J Comput Nonlinear Dyn* 2016;11(1):011012.
- [26] Yi M, Huang J. Wavelet operational matrix method for solving fractional differential equations with variable coefficients. *Appl Math Comput* 2014;230:383–94.
- [27] Goswami P, Alqahtani RT. On the solution of local fractional differential equations using local fractional laplace variational iteration method. *Math Probl Eng* 2016.
- [28] Jafari H, Jassim HK. Numerical solutions of telegraph and laplace equations on cantor sets using local fractional laplace decomposition method. *Int J Adv Appl Math Mech* 2015;2(3):144–51.
- [29] Atangana A, Baleanu D. New fractional derivatives with nonlocal and non-singular kernel: theory and application to heat transfer model. *Therm Sci* 2016;20(2):763–9.
- [30] Gómez-Aguilar JF. Irving-mullineux oscillator via fractional derivatives with mittag-leffler kernel. *Chaos, Solitons Fractals* 2017;95:179–86.
- [31] Alkahtani BST. Chua's circuit model with atangana-baleanu derivative with fractional order. *Chaos, Solitons Fractals* 2016;89:547–51.
- [32] Sheikh NA, Ali F, Saqib M, Khan I, Jan SAA. A comparative study of atangana-baleanu and caputo-fabrizio fractional derivatives to the convective flow of a generalized casson fluid. *Eur Phys J Plus* 2017;132(1):54.
- [33] Li C, Chen G. Chaos and hyperchaos in the fractional-order rössler equations. *Physica A* 2004;341:55–61.
- [34] Bhowry AH, Zaky MA. An improved collocation method for multi-dimensional space-time variable-order fractional schrödinger equations. *Appl Numer Math* 2017;111:197–218.
- [35] Valério D, Da Costa JS. Variable-order fractional derivatives and their numerical approximations. *Signal Process* 2011;91(3):470–83.
- [36] Atangana A. On the stability and convergence of the time-fractional variable-order telegraph equation. *J Comput Phys* 2015;293:104–14.
- [37] Sun HG, Chen W, Wei W, Chen YQ. A comparative study of constant-order and variable-order fractional models in characterizing memory property of systems. *Eur Phys J Special Topics* 2011;193(1):185–92.
- [38] Cooper GRJ, Cowan DR. Filtering using variable order vertical derivatives. *Comput Geosci* 2004;30(5):455–9.
- [39] Moghaddam BP, Machado JAT. A stable three-level explicit spline finite difference scheme for a class of nonlinear time variable order fractional partial differential equations. *Comput Math Appl* 2016.
- [40] Atangana A, Botha JF. A generalized groundwater flow equation using the concept of variable-order derivative. *Bound Value Probl* 2013;2013(1):53.
- [41] Yaghoobi S, Moghaddam BP, Ivaz K. An efficient cubic spline approximation for variable-order fractional differential equations with time delay. *Nonlinear Dyn* 2017;87(2):815–26.
- [42] Atangana A, Alqahtani RT. Stability analysis of nonlinear thin viscous fluid sheet flow equation with local fractional variable-order derivative. *J Comput Theor Nanosci* 2016;13(5):2710–17.
- [43] Moghaddam BP, Yaghoobi S, Machado JT. An extended predictor-corrector algorithm for variable-order fractional delay differential equations. *J Comput Nonlinear Dyn* 2016;11(6):061001.
- [44] Romero-Ugalde HM, Corbier C. Robust estimation of balanced simplicity-accuracy neural networks-based models. *J Dyn Syst Meas Control* 2016;138(5):051001.
- [45] Cybenko G. Approximation by superpositions of a sigmoidal function. *Math Control, Signals, Systems (MCSS)* 1989;2(4):303–14.
- [46] Huang GB, Zhu QY, Siew CK. Extreme learning machine: theory and applications. *Neurocomputing* 2006;70(1):489–501.

- [47] Romero-Ugalde HM, Carmona JC, Reyes-Reyes J, Alvarado VM, Corbier C. Balanced simplicity-accuracy neural network model families for system identification. *Neural Comput Appl* 2015;26(1):171–86.
- [48] Romero-Ugalde HM, Carmona JC, Alvarado VM, Reyes-Reyes J. Neural network design and model reduction approach for black box nonlinear system identification with reduced number of parameters. *Neurocomputing* 2013;101:170–80.
- [49] Das T, Kar IN. Design and implementation of an adaptive fuzzy logic-based controller for wheeled mobile robots. *IEEE Trans Control Syst Technol* 2006;14(3):501–10.
- [50] Chen M, Ge SS, How BVE. Robust adaptive neural network control for a class of uncertain MIMO nonlinear systems with input nonlinearities. *IEEE Trans Neural Networks* 2010;21(5):796–812.
- [51] Krizhevsky A, Sutskever I, Hinton GE. Imagenet classification with deep convolutional neural networks. In: Advances in neural information processing systems; 2012. p. 1097–105.
- [52] Ciregan D, Meier U, Schmidhuber J. Multi-column deep neural networks for image classification. In: Computer Vision and Pattern Recognition (CVPR), 2012 IEEE Conference; 2012. p. 3642–9.
- [53] Qu H, Liu X. A numerical method for solving fractional differential equations by using neural network. *Adv Math Phys* 2015.
- [54] Jafarian A, Mokhtarpour M, Baleanu D. Artificial neural network approach for a class of fractional ordinary differential equation. *Neural Comput Appl* 2016;1:1–9.
- [55] Raja MAZ, Khan JA, Qureshi IM. A new stochastic approach for solution of riccati differential equation of fractional order. *Ann Math Artif Intell* 2010;60(3):229–50.
- [56] Raja MAZ, Khan JA, Qureshi IM. Solution of fractional order system of bagley-torvik equation using evolutionary computational intelligence. *Math Probl Eng* 2011;2011:675075.
- [57] Raja MAZ, Manzari MA, Samar R. An efficient computational intelligence approach for solving fractional order riccati equations using ANN and SQP. *Appl Math Model* 2015;39:3075–93.
- [58] Kashkaria BS, Syam MI. Evolutionary computational intelligence in solving a class of nonlinear volterra-fredholm integro-differential equations. *J Comput Appl Math* 2017;311:314–23.
- [59] Pakdaman M, Ahmadian A, Effati S, Salahshour S, Baleanu D. Solving differential equations of fractional order using an optimization technique based on training artificial neural network. *Appl Math Comput* 2017;293:81–95.
- [60] Costa M, Braga AP, De Menezes BR. Improved generalization learning with sliding mode control and the levenberg-marquadt algorithm. In: Neural Networks, 2002. SBRN 2002. Proceedings. IEEE, VII Brazilian Symposium on; 2002. p. 44–8.
- [61] Odibat ZM, Momani S. An algorithm for the numerical solution of differential equations of fractional order. *J Appl Math Inform* 2008;26:15–27.
- [62] Saadatmandi A, Dehghan M. A new operational matrix for solving fractional-order differential equations. *Comput Math Appl* 2010;59(3):1326–36.
- [63] Ma S, Xu Y, Yue W. Numerical solutions of a variable-order fractional financial system. *J Appl Math* 2012;2012.
- [64] Li C, Tao C. On the fractional adams method. *Comput Math Appl* 2009;58(8):1573–88.
- [65] Yalcin ME, Suykens JA, Vandewalle J, Özoguz S. Families of scroll grid attractors. *Int J Bifurcation Chaos* 2002;12(01):23–41.